Neutralization of zoonotic simian foamy viruses: genotype-specific epitopes within the receptor-binding domain

Lasse Toftdal Dynesen[a], Ignacio Fernandez[b], Youna Coquin[a], Manon Delaplace[a], Thomas Montange[a], Richard Njouom[c], Chanceline Bilonga-Ndongo[d], Felix A. Rey[b], Antoine Gessain[a], Marija Backovic[b], and Florence Buseyne[a,*]

[a]Institut Pasteur, Université Paris Cité, CNRS UMR3569, Unité d'Epidémiologie et Physiopathologie des Virus Oncogènes, 75015 Paris, France

[b]Institut Pasteur, Université Paris Cité, CNRS UMR3569, Unité de Virologie Structurale, 75015 Paris, France

[c]Centre Pasteur du Cameroun, Yaoundé, Cameroon

[d]Ministère de la Santé Publique, Yaoundé, Cameroon

[*]corresponding author

Abstract

Simian foamy viruses (SFVs) are retroviruses that are frequently cross-transmitted to humans. SFVs establish life-long infection in their human hosts, with the persistence of replication-competent virus. Zoonotic SFVs do not induce severe pathology and are not transmitted between humans. Infected individuals develop potent neutralizing antibodies (nAbs) that targets the SFV envelope protein (Env). Env carries a variable region that defines two SFV genotypes and is the exclusive target of nAbs. However, its antigenic determinants are not understood. Here, we characterized nAbs from SFV-infected individuals living in Central Africa. The nAbs target conformational epitopes within two major antigenic areas located at the Env apex: One mediates the interaction between Env protomers to form Env trimers and one harbors several determinants of Env binding to susceptible cells. One binding determinant is genotype-specific. We propose a model integrating structural, genetic, functional, and immunological knowledge on the SFV receptor binding domain.

30 # Introduction

31 Foamy viruses (FVs) are the most ancient of retroviruses [1, 2]. Simian foamy viruses (SFVs) are
32 widespread in nonhuman primates (NHPs), replicate in the buccal cavity, and are transmitted to
33 humans mostly through bites by infected NHPs [2-4]. Such cross-species transmission events currently
34 occur in Asia, Africa, and the Americas. Most individuals known to be infected with zoonotic SFV live
35 in Central Africa, the region at the epicenter of the emergence of HIV-1 and HTLV-1 from their simian
36 reservoirs. In their human hosts, SFVs establish a life-long persistent infection associated with
37 subclinical pathophysiological alterations [5, 6]. Thus far, neither severe disease nor human-to-human
38 transmission have been described, suggesting efficient control of SFV replication and transmission in
39 humans.

40 SFV infection elicits envelope (Env)-specific neutralizing antibodies (nAbs) that block the entry of viral
41 particles into susceptible cells *in vitro* [7]. Although they do not block cell-to-cell infection *in vitro*,
42 antibodies prevent cell-associated SFV transmission by transfusion in monkeys [8, 9]. SFV Env is cleaved
43 into three subunits, the leader peptide (LP), the surface subunit (SU), which binds to cells, and the
44 transmembrane (TM) subunit, which carries out fusion. In several SFV species, there are two variants
45 of the *env* gene, defining two genotypes [10-12]. The two variants differ in a discrete region encoding
46 250 residues, named SUvar, located at the center of the SU and overlapping with most of the receptor-
47 binding domain (RBD) [13]. The RBD is thus bimorphic and the exclusive target of genotype-specific
48 nAbs [7].

49 We have determined the RBD structure, which we describe in a co-submitted paper [14]. Here, we
50 present the epitopic sites that were concomitantly defined by the use of plasma samples from SFV-
51 infected African hunters. These individuals were infected by SFV of gorilla origin through bites [3]. We
52 have previously described the infecting strains, *ex vivo* blood target cells, antibody response, and
53 medical status of these individuals [5-7, 9, 11, 15, 16]. We expressed the SU as a soluble recombinant
54 protein that competes with SU present on viral vector particles for binding to plasma nAbs in a
55 neutralization assay. We defined the regions targeted by the nAbs using mutant SU protein modified
56 at the glycosylation sites [17], RBD functional subregions [13], genotype-specific sequences that
57 present properties of B-cell epitopes, and structural information [14]. Finally, we tested whether
58 immunodominant epitopes recognized by nAbs are involved in SU binding to and viral entry into
59 susceptible cells.

60

61 # Results

62 ## Infrequent binding of plasma antibodies to linear epitopes located on the SU variable
63 domain

64 We started the epitope mapping project by screening plasma samples for binding to 37 synthetic
65 peptides spanning the SUvar domain from three viral strains (Fig. 1, Supplementary Tables 1 and 2,
66 Supplementary Fig. 1). By ELISA, seven of 17 (41%) plasma samples from SFV-infected individuals reacted
67 against at least one peptide; five locations represented by peptides with GI and/or GII sequences were
68 recognized by at least one plasma sample (Fig. 2). In comparison, 76%, and 71% of plasma samples
69 displayed binding activity against immunodominant viral peptides used as positive controls (see
70 Materials and Methods). Plasma antibodies bound to GI and/or GII peptides irrespective of the SFV
71 genotype against which they were raised. In conclusion, the binding study showed that most SFV-
72 specific antibodies do not recognize genotype-specific linear epitopes.

73 ## SFV SU protein competes with the virus for binding to nAbs

74 We sought to define nAb epitopes by performing neutralization assays in the presence of recombinant
75 SU protein that competes with the SU within Env present at the surface of foamy viral vector (FVV)
76 particles. While wildtype (WT) SU bound to the nAbs, allowing cell infection to proceed, SU mutants
77 with altered nAb epitopes did not (Fig. 3A and 3B). We tested several recombinant Env and SU
78 expression constructs, of which the production level and stability varied according to the genotype:
79 Gorilla genotype II (GII) Env-derived constructs were expressed at high levels, whereas gorilla genotype
80 I (GI) Env-derived counterparts were poorly expressed and aggregated (Supplementary Fig. 2A). The
81 immunoglobulin Fc domain acts as a secretion carrier for the SU, giving the construct high stability.
82 Such chimeric proteins - referred to as immunoadhesins – have been used to produce soluble SFV SU
83 [13]. The GI SU immunoadhesin was expressed at insufficient levels, but we readily produced the
84 chimpanzee genotype I (CI) and GII SU immunoadhesins. We therefore studied epitopes recognized by
85 GII-specific nAbs with the GII immunoadhesin (referred to as ^{GII}SU for the WT sequence) and those
86 recognized by GI-specific nAbs with the CI immunoadhesin (^{CI}SU), as allowed by the frequent cross-
87 neutralization of gorilla and chimpanzee strains belonging to the same genotype [7] and CI and GI
88 SUvar sequence identity of 70% [11].

89 We validated the competition strategy with genotype-matched and mismatched immunoadhesins (Fig.
90 3, Supplementary Tables 3 and 4). We tested plasma samples from gorilla SFV-infected hunters at the
91 dilution required for 90% reduction of FVV infectivity (IC_{90}) to allow Env-specific antibody saturation
92 by the competitor immunoadhesin. Thus, plasma samples were tested at the same nAb concentration
93 and responses from different individuals could be compared. We incubated immunoadhesins with

94 plasma samples before addition to a FVV expressing the matching envelope protein and titration of
95 residual infectivity. Both ^{CI}SU and ^{GII}SU blocked the action of nAbs present in genotype-matched plasma
96 samples in a concentration-dependent manner but failed to block the activity of genotype-mismatched
97 samples (Fig. 3C). Importantly, the immunoadhesins did not affect SFV entry (Fig. 3D, [18]), allowing
98 their use as competitors for binding to nAbs in an infectivity assay. The unrelated MLV SU construct
99 (^{MLV}SU) had no impact on either the neutralizing activity of plasma samples or SFV infectivity (Fig. 3C
100 and 3D). We titrated 12 samples against matched ^{CI}SU and ^{GII}SU, including one from a coinfected
101 individual which was tested against both immunoadhesins, leading to 13 sample-immunoadhesin pairs
102 tested. Immunoadhesin's effect on nAb can be described by its affinity and by the fraction of plasma
103 nAb blocked. The IC_{50}, a measure of affinity, ranged between 3.3 and 12.6 nM for ^{CI}SU and 2.9 and 12.5
104 nM for ^{GII}SU, depending on the plasma sample (Fig. 3E). Taking FVV treated with ^{MLV}SU without plasma
105 as a reference value for full infectivity (100%), ^{CI}SU and ^{GII}SU restored the infectivity of plasma-treated
106 FVV to between 56% and 94% of infectivity. This value is referred to as maximum infectivity (MaxI) and
107 quantifies the proportion of nAb blocked by the immunoadhesion (Fig. 3B and 3F). We used the values
108 from at least five independent experiments to calculate the IC_{50} and MaxI threshold values to define
109 the nAb blocking activity of mutated recombinant proteins as being significantly different from that of
110 WT SU (Fig. 3B).

111 We evaluated the impact of SU oligomerization and mammalian-type glycosylation on its capacity to
112 block nAbs by testing the following constructs: SU monomers produced in mammalian and insect cells,
113 trimeric Env ectodomains produced in insect cells, and dimeric SU (i.e., immunoadhesin) produced in
114 mammalian cells. All had the same capacity to block the nAbs (Supplementary Fig. 2B). Therefore, we
115 used the only recombinant proteins available for both genotypes, the SU immunoadhesins. We first
116 studied GII-specific nAbs using ^{GII}SU before testing GI-specific nAbs using ^{CI}SU.

117 Certain nAbs target glyco-epitopes

118 The GII SUvar domain carries seven of the 11 SU glycosylation sites (Fig. 4A and 4B). We assessed
119 whether these glycans are recognized by nAbs or whether they shield epitopes from nAb recognition.
120 We produced ^{GII}SU in the presence of the mannosidase inhibitor kifunensine, which prevents complex-
121 type glycan addition, or treated it with endo-H to remove all glycans. The absence of complex glycans
122 had no impact on nAb blockade by ^{GII}SU (Fig. 4C), confirming data obtained with GII Env constructs
123 expressed in insect cells, which also lack complex glycans (Supplementary Fig. 2). By contrast, the removal
124 of all glycans decreased nAb blockade and protein titration showed lower affinity for the nAbs present
125 in three out of four plasma samples (Fig. 4D). Endo-H treatment did not induce protein aggregation
126 (Supplementary Fig. 4) but may have a global effect on the SU affecting SFV-specific nAbs. Conversely,

127 glycans did not shield major nAb epitopes on SFV Env, as their removal did not enhance nAb blockade
128 in the samples tested.

129 The N10 glycosylation site is located at different positions for the two genotypes and may be part of a
130 potential epitopic region (N422/N423 on GI-D468/CI-PFV strains, N411 on the GII-K74 strain). The N10
131 glycosylation knock-down mutant (^{GII}ΔN10) was as efficient as ^{GII}SU in blocking nAbs from all plasma
132 samples (Fig. 4E). N10 belongs to a stretch of seven genotype-specific residues that were replaced by
133 those from the GI-D468 strain. The chimeric protein (^{GII}swap407) blocked nAbs as efficiently as ^{GII}SU
134 for three samples and showed decreased affinity against nAbs for one sample (Fig. 4F). Thus, GII-
135 specific nAbs occasionally target the N10 glycosylation site.

136 To identify other glycosylation sites targeted by nAbs, we knocked them down one by one, except for
137 N8, which is critical for SU expression [17]. The ^{GII}ΔN7' mutant showed reduced capacity to block nAbs
138 from five of the seven samples (Fig. 4J). ^{GII}ΔN5 and ^{GII}ΔN9 showed reduced capacity to block nAbs from
139 one or two plasma samples (Fig. 4G and 4K). Knock down of N6 and N7 had no impact (Fig. 4H and 4I).
140 Overall, our data support that most glycans are not part of glyco-epitopes, except those at the N7'
141 glycosylation site.

142 SFV-specific nAbs target loops at the RBD apex

143 Next, we aimed to locate nAb epitopes on the SU subdomains involved in binding to susceptible cells
144 [13]. Two regions of the RBD were identified as being essential for binding (RBD1 and RBD2) and the
145 region in between (RBDj) could be deleted without fully compromising cell binding (Fig. 1A, 1C, 5A and
146 5B). The SUvar region encompasses RBD1 (except its first 16 N-term residues), RBDj, and the seven N-
147 terminal residues of RBD2 (Fig. 1B, 1D). We first constructed a mutant immunoadhesin with RBDj
148 deleted. ^{GII}ΔRBDj was highly impaired in blocking nAbs from three individuals: the IC_{50} values were
149 above the highest concentration tested (200 nM) and the MaxI values were close to 10%, the value of
150 plasma samples incubated with the irrelevant ^{MLV}SU (Fig. 5C). By contrast, ^{GII}ΔRBDj blocked nAbs from
151 the BAD551 plasma sample as efficiently as ^{GII}SU.

152 Then, we used the recently discovered RBD structural elements. In the lower subdomain, the main
153 candidate epitopic region was the heparan sulfate glycosaminoglycan binding site (HBS). The GII Env
154 ectodomain mutated on HBS residues (^{GII}K342A/R343A or ^{GII}R356A/R369A, [14]) blocked nAbs from
155 three samples as efficiently as their WT counterpart and showed lower affinity for the MEBAK88
156 plasma sample (Fig. 5D and 5E). Thus, nAb activity is modestly affected by mutated HBS residues.

157 The X-ray structure of the RBD showed that four loops emanate from the upper domain [14]. L1 is
158 shielded at the center of the trimer and is probably not accessible to nAbs, whereas L2 (276-281), L3

159 (416-436), and L4 (446-453) are exposed to solvent, mobile, and therefore considered to be candidate
160 epitopic regions. Furthermore, L3 and L4 are located in the RBDj region, which is a major target of nAbs
161 (Fig. 5C). We deleted the loops individually (Fig. 5F-H). ^{GII}ΔL3 blocked all GII-specific samples but one,
162 although with lower affinity. ^{GII}ΔL2 and ^{GII}ΔL4 showed plasma-dependent effects, with three patterns:
163 (1) full activity (such as against BAD551) (2), full loss or a strong reduction of activity (for example,
164 against BAK133), (3) or reduction of the MaxI with unchanged affinity (such as MEBAK88). The last
165 pattern probably reflects the presence of nAbs targeting different epitopes within the same plasma
166 sample, some epitopes being altered on mutant immunoadhesins while others are not.

167 Even though L2, L3, and L4 are mobile in the structure of the RBD monomer [14], the plasma samples
168 did not recognize synthetic peptides spanning these loops (Supplementary Fig. 5), indicating that they
169 may be part of conformational epitopes. Overall, we show that nAbs from most samples target
170 conformational epitopes at the RBD apex, some being carried by L2, L3, and L4.

171 SFV-specific nAbs target the base of the SUvar region

172 Before the 3D structure was available, we used the insertion of N-linked glycosylation sequences
173 (NXS/T) to disrupt potential epitopes. We selected seven genotype-specific sequences predicted to
174 have a disordered secondary structure or to contain a B-cell epitope and built mutant immunoadhesins
175 with a glycosylation site inserted in the targeted sequence (Fig. 6A, 6B, Supplementary Table 5). Four of
176 the seven glycans were inserted in the upper subdomain and resulted in decreased affinity against
177 certain plasma nAbs: $^{GII}426_{glyc}$ in L3, $^{GII}450_{glyc}$ in L4, $^{GII}459_{glyc}$ after L4, and $^{GII}485_{glyc}$ in RBDj (Fig. 6C-F).
178 $^{GII}263_{glyc}$ had no or only a modest effect on nAb activity, which is consistent with its location at the
179 center of the trimer (Fig. 6G, [14]). Overall, glycan insertions at five sites of the RBD upper subdomain
180 confirmed its frequent recognition by nAbs.

181 One immunoadhesin with glycans inserted in the lower RBD subdomain ($^{GII}351_{glyc}$) showed a strongly
182 reduced capacity to block the nAbs (Fig. 6H). The modified residue is located on a solvent-exposed loop
183 at the base of the SUvar region (aa 345-353) (Fig. 6B and 6B'). $^{GII}351_{glyc}$ was the first mutant to indicate
184 that nAbs recognize a region of the RBD to which no function has yet been attributed. We therefore
185 focused the following experiments on this novel epitopic region.

186 As $^{GII}351_{glyc}$ was prone to aggregation (Supplementary Fig. 4H), we produced a second batch, half of which
187 was purified by affinity chromatography (standard protocol) and the other half further purified by size
188 exclusion chromatography (SEC) to eliminate aggregates. Both $^{GII}351_{glyc}$ preparations were unable to
189 block nAbs from the plasma samples (Supplementary Fig. 6A-E). Glycan insertion at an adjacent position
190 in $^{GII}350_{glyc}$ led to the loss of nAb blockade and reduced aggregation (Fig. 6I). The GII 345-353 loop is
191 one residue shorter than that of the GI-D468 and CI-PFV strains (Fig. 6B'). The mutant immunoadhesin

192 with an extra E at position 349 (^{GII} 349$_{+E}$) showed a strongly reduced capacity to block the nAbs (Fig.
193 6J). We replaced the seven GII residues by the eight residues from the GI-D468 strain; ^{GII}swap345
194 showed a reduced ability to block nAbs from five of the seven plasma samples (Fig. 6K). By contrast,
195 swapping the α3-helix located N-terminal to the loop (^{GII}swap333) had no impact on the capacity to
196 block the nAbs (Fig. 6L). Finally, we tested the substitution of residues on the α8-helix facing the 345-
197 353 loop; ^{GII}E502A and ^{GII}L505N showed a reduced capacity to block the nAbs (Fig. 6M-N). Overall, these
198 experiments define the 345-353 loop and adjacent α8-helix as a major epitopic region on GII RBD.

199 GI and GII-specific nAbs target different epitopes

200 We applied a similar strategy using GI-specific plasma samples and ^{CI}SU harboring the mutations with
201 the greatest impact on GII-specific epitopes. We present these data with a comparison with those
202 obtained with the GII-specific samples (Fig. 7, blue symbols over light red lines). GI-specific nAbs
203 targeted glycans removed by endo-H but not complex glycans and did not recognize N10, for which
204 the presence is genotype-specific (Fig. 7A-7C). We could not test the recognition of N7', as it is absent
205 from the CI-PFV strain.

206 The most striking difference between GI and GII epitopes was around residue 350: in sharp contrast to
207 ^{GII}351$_{glyc}$ (Fig. 6H) and ^{GII}350$_{glyc}$ (Fig. 6I), ^{CI}350$_{glyc}$ fully blocked GI-specific nAbs (Fig. 7D). Neither ^{CI}ΔRBDj
208 nor ^{CI}ΔL3 proteins blocked the nAbs (Fig. 7E and 7G). Thus, L3 is more important for GI- than GII-specific
209 nAbs. Indeed, ^{GII}ΔL3 blocked GII-specific nAbs, although with lower affinity than ^{GII}SU. ^{CI}ΔL2 and ^{CI}ΔL4
210 showed sample-dependent effects, as their GII counterparts (Fig. 7F and 7H). ^{CI}463$_{glyc}$ blocked GI-specific
211 nAbs, with a reduced MaxI (Fig. 7I), indicating that a fraction of GI-specific nAbs was not blocked,
212 whereas the other was blocked as efficiently as by ^{CI}SU. The corresponding ^{GII}459$_{glyc}$ mutant blocked
213 GII-specific nAbs, but with lower affinity than ^{GII}SU (Fig. 6E). Overall, nAbs from GI- and GII-specific
214 plasma samples target different epitopes.

215 The mutations on the SU immunoadhesins may have induced epitope-specific or nonspecific
216 conformational changes. The RBDj deletion had a likely epitope-specific effect on the GII backbone, as
217 ^{GII}ΔRBDj retained its capacity to block one sample containing nAbs that preferentially targeted epitopes
218 outside the RBDj (Fig. 5C). However, ^{CI}ΔRBDj and ^{CI}ΔL3 did not display any nAb blocking activity. Thus,
219 we confirmed the results using chimeric immunoadhesins: ^{GII}swapRBDj (i.e., GI RBDj in ^{GII}SU) blocked
220 nAbs from the four anti-GI plasma samples with a similar or modestly reduced capacity relative to that
221 of ^{CI}SU (Fig. 7J), whereas ^{GII}SU had no blocking activity (Fig. 7K). ^{CI}swapL3 (GII L3 in ^{CI}SU) did not block
222 the nAbs (Fig. 7L). These data suggest that either GI-specific nAbs recognize the L3 loop or that the L3
223 loop requires a matching interaction to adopt its native conformation.

Human plasma samples contain nAbs targeting a variable number of epitopic regions

The effect of the mutant SU on each plasma sample can be summarized as recognition similar to that as for WT SU, recognition with a reduced affinity (i.e., increased IC_{50}), blocking a smaller fraction of nAbs than WT SU (i.e., reduced MaxI), or having both effects (Fig. 8). We grouped the most relevant mutants according to their location: the RBD apex, the 345-353 loop, and the N7' region. We tested the recognition of the N7' region by GII-specific samples only. This summary highlights the two genotype-specific and immunodominant epitopic regions that we identified: loop 345-353 on ^{GII}SU (Fig. 8A) and L3 on ^{CI}SU (Fig. 8B). Within the RBD apex, four mutant immunoadhesins correspond to different epitopic sites (L2, L3, L4, and 459/463^{glyc}). GI-specific plasma samples contained nAbs focused on a single subdomain (such as BAK55 and ^{CI}L3) or epitopes on up to four sites (BAD348 and BAK132). Similarly, GII-specific plasma samples presented interindividual variations in their specificity. We examined the sequence of the identified epitopes and found that all were conserved on the SFV strains infecting individuals from this study or circulating in Central Africa (Supplementary Fig. 7). Overall, we identified three immunodominant epitopic regions (RBD apex, 345-353 loop, and N7' region), of which the sequences are conserved within each genotype. We provide evidence that SFV-infected individuals have nAbs that target several epitopes and recognize epitopes that differ between individuals.

Functional studies

Protein binding to susceptible cells

All immunoadhesins used for epitope mapping were tested for their capacity to bind to human HT1080 cells, which are highly susceptible to gorilla and chimpanzee SFVs [15] (Fig. 9A, Supplementary Fig. 8). Immunoadhesin binding was enhanced after glycan removal, possibly through reduced steric hindrance. Deletion of the RBDj reduced binding to susceptible cells, while one-by-one deletion of loops L2, L3, and L4 abolished it. We observed genotype-specific differences; the RBDj deletion had a stronger impact on GII than on CI immunoadhesins (6- vs. 2.5-fold reduction). Conversely, glycan insertion after L4 had only a moderate impact on the GII immunoadhesin ($^{GII}459_{glyc}$, 6-fold reduction) but abolished binding of the CI immunoadhesin ($^{CI}463^{glyc}$,≈100-fold reduction). In the 345-353 loop, glycan insertion strongly affected the binding of GII immunoadhesins ($^{GII}350_{glyc}$ and $^{GII}351_{glyc}$, ≈50-fold reduction), but there was no effect on CI immunoadhesins, mirroring the recognition by the nAbs. Overall, our data suggest that certain residues involved in cell binding may be genotype-specific.

The binding data were also considered for the interpretation of nAb blocking experiments. The mutant immunoadhesins that retained their capacity to bind cells were considered to likely be properly folded and loss of nAb blockade could be considered as being due to mutation of the epitope. Overall, a single

256 mutated adhesins failed to bind cells and block the nAbs from all samples tested and related data are
257 not presented.

258 The epitopic regions targeted by nAbs are involved in viral infectivity

259 We then tested the impact of RBDj and loop deletions in the context of FVVs. We produced FVVs with
260 Env mutants corresponding to the immunoadhesins most affected in blocking genotype-specific nAbs
261 (i.e., ΔRBDj and ΔL3 CI-PFV, ΔRBDj, ΔL2, and ΔL4 GII-K74 Env). The quantity of FVV particles carrying
262 deletions was strongly reduced, over 1000-fold for CI-PFV ΔRBDj, over 100-fold for CI-PFV ΔL3 and GII-
263 K74 ΔRBDj, and over 50-fold GII-K74 ΔL2 and ΔL4 (Fig. 9B), despite all mutant Env being expressed in
264 transfected cells (Supplementary Fig. 9). Moreover, none of the FVVs with mutant Env were infectious
265 (Fig. 9C). However, most bound to susceptible cells at levels 2 to 4-fold below those of FVVs with WT
266 Env, except the CI-PFV ΔRBDj mutant, for which the binding was reduced ≈ 30-fold) (Fig. 9D). In
267 conclusion, the regions from the upper RBD subdomain targeted by nAbs are required for viral
268 infectivity independently of their capacity to bind to susceptible cells.

269 Three-dimensional map of epitopic regions

270 We built a model integrating the current knowledge on Env structure, genetic variability, function, and
271 our findings on the recognition by nAbs (Fig. 10). According to our model for the arrangement of the
272 RBD within the trimeric Env, the RBD occupies the space at the top of Env spike [14, 19]; each RBD has
273 two subdomains, referred to as upper and lower [14] (Fig. 10A). The genotype-specific SUvar region is
274 targeted by nAbs [7, 11, 12] and comprises the entire upper RBD subdomain ($SUvar^{Up}$) and one third
275 of its lower subdomain ($SUvar^{Lo}$) (Fig. 10B). $SUvar^{Lo}$ wraps around a stem formed by the conserved part
276 of the RBD (SUcon region). The functionally defined bipartite RBD [13] could be located as follows:
277 RBD1 forms half of the $SUvar^{Up}$ and the $SUvar^{Lo}$ region wrapping around the conserved RBD2, while
278 the RBDj forms the top of $SUvar^{Up}$.

279 Here, we show that nAbs recognize the three solvent-exposed loops on $SUvar^{Up}$ (Fig. 10D). We also
280 identified mutations located C-terminal ($^{GII}459_{glyc}$ and $^{CI}463_{glyc)}$ that may affect nAb binding or the SU
281 folding. For $SUvar^{Lo}$, we show the 345-353 loop to be an immunodominant epitope exclusively
282 recognized by GII-specific nAbs and that it has a role in binding to cells. The glycosylation site N7' had
283 the greatest impact on the nAbs. It is located at the opening of the cavity in which the essential N8
284 glycan is buried [14]. Of note, the glycan inserted in $^{GII}485_{glyc}$ may interfere with N8 function and/or
285 accessibility to nAbs. $SUvar^{Lo}$ comprises the HBS, which was not frequently recognized. In conclusion,
286 the nAbs bound to the loops on $SUvar^{Up}$ might interfere with trimer integrity or the conformational
287 changes required for the triggering of fusion, whereas those that bound to $SUvar^{Lo}$ may prevent viral
288 attachment and/or binding.

289 ## Discussion

290 Here, we demonstrate that SFV GII-specific nAbs raised by infected humans recognize two antigenic
291 regions in the genotype-specific region of the SU and that GI-specific nAbs target at least one of these
292 regions. Based on previous knowledge [13, 19], the X-ray structure presented in the co-submitted
293 paper [14], and our functional data, the SFV-specific nAbs most likely target sites involved in either Env
294 trimer formation or cell binding.

295 We identified conformational epitopes only, despite several attempts to capture linear epitopes using
296 peptides (Fig. 2, Supplementary Fig. 5 and [20]). Our data are consistent with the low reactivity of NHP
297 and human immune sera to denatured Env in immunoblot assays, which contain Abs that bind to native
298 Env in radio-immunoprecipitation and neutralization assays [21-24]. Linear epitopes are usually
299 located in mobile regions of the polypeptide chains. Such mobile segments are absent from the RBD
300 lower subdomain formed by the compact assembly of α-helices and β-sheets [14]. In RBD monomers,
301 the upper subdomain loops appear to be mobile, but inter-protomer interactions probably impose
302 specific conformations in full-length Env. The loops likely form a number of discontinuous epitopes; L2
303 and L4 are in proximity in the monomer and L3 and L4 in the trimer [14].

304 Twelve plasma samples were used in this study, including one from an individual infected by strains
305 belonging to both genotypes. Overall, the epitopic regions were recognized by all or most donors and
306 can be considered to be immunodominant (Fig. 8). Importantly, within each genotype, sequences from
307 the epitopic regions were identical among SFV strains infecting the studied individuals and those
308 circulating in the same geographical area. This observation is consistent with the genetic stability of
309 SFV [25]. The use of polyclonal plasma samples was key to providing a global picture of nAbs raised
310 upon infection with zoonotic SFV, but only epitopes recognized by a significant fraction of plasma
311 antibodies can be detected. Thus, future studies may identify subdominant epitopes and provide a
312 more precise definition of those that are immunodominant.

313 Immunoadhesins fully blocked nAbs from certain samples. However, for most tested samples, the
314 infectivity was maintained but at levels lower than those observed for FVVs not exposed to plasma
315 samples (Fig. 3). The heterogeneous glycosylation of the immunoadhesins could explain the partial
316 blockade of nAbs [23], as proposed for the incomplete neutralization of HIV [26-29]. The SU
317 antigenicity of soluble monomeric proteins probably differed from those contained within viral
318 particles due to the lack of the intra- and interprotomer interactions that form quaternary structures.
319 Thus, our data identify nAb epitopes presented on the monomeric SU domain and indirectly suggest
320 the existence of quaternary epitopes.

321 We have provided experimental evidence for the targeting of different epitopes by nAbs raised after
322 infection by the two SFV genotypes. The RBD fold from different genotypes and FV from different host
323 species is highly conserved [14]. In superinfection-resistance experiments, the CI Env inhibited entry
324 from genotype II strains, indicating that SFV from different genotypes share the use of at least one
325 molecule for entry into target cells; this molecule could act as an attachment factor or receptor [30].
326 The SUvar^{Up} domain was recognized by both GI- and GII-specific nAbs and the SUvar^{Lo} by GII-specific
327 nAbs only. GI-specific nAbs may, nevertheless, recognize epitopes on SUvar^{Lo} that are yet to be
328 identified. Indeed, the biochemical properties of GI Env protein resulted in low expression and protein
329 aggregation. Therefore, we used an SU from chimpanzee genotype I SFV to map epitopes recognized
330 by antibodies induced by a gorilla genotype I SFV. We previously reported that plasma samples cross-
331 neutralize both SFV species, with a strong correlation between nAb titers; however, nAb titers were
332 globally higher against the GI than CI strain [7]. Thus, we may have missed a number of GI-specific
333 epitopes.

334 Relative to other viruses, SFV-specific nAbs target a limited region on Env, i.e., they do not recognize
335 epitopes on the TM nor non-RBD sites of the SU [31-33]. Based on the inhibition mechanisms described
336 for other viruses [33], we can propose a number of possible modes of action. The targeting of RBD
337 loops by nAbs may prevent the fusogenic conformational transition and exposure of the fusion
338 peptide, which is located at the center of the trimer and shielded by the RBD, as visualized on viral
339 particles [19]. It is possible that certain loop-specific nAbs bind several protomers, as described for
340 HIV- and Ebola-specific nAbs [34, 35]. An alternative neutralization mechanism could be the targeting
341 of epitopes located close to the protomer interface, resulting in trimer disruption, as described for HIV-
342 and Flu-specific nAbs [36, 37].

343 Many nAbs interfere with particle binding to susceptible cells. The existence of a *bona fide* receptor
344 for SFV is yet to be demonstrated. Consequently, the molecular determinants of Env binding to
345 susceptible cells within SUvar^{Lo} are still only roughly defined. Certain nAbs recognize attachment
346 factors, such as an HBS on SARS-CoV2 spike [38]. The SFV HBS is a patch of residues located in SUvar^{Lo}.
347 The mutants deficient for HS binding efficiently blocked most plasma samples, indicating that HBS is
348 either not a major nAb target or that the antigenicity of these mutants is preserved. Of note, the N7'
349 site located in the vicinity of HBS was recognized. All immunoadhesins designed to map potential B-
350 cell epitopes were tested for their capacity to bind susceptible cells. SU from the two genotypes
351 differed in certain residues involved in cell binding. Most notably, nAbs recognizing the 345-353 loop
352 may prevent GII Env binding, whereas the loop on GI Env is not involved in cell binding and is not
353 targeted by nAbs (Fig. 9). This last observation highlights, for the first time, genotype-specific

354 differences in SFV binding to susceptible cells and could be a starting point for further studies on
355 identifying attachment factors and receptors for SFV.

356 Our choice of a functional strategy to map the epitopes targeted by nAbs proved to be critical due to
357 the lack of linear epitopes. Overall, the use of human samples and soluble SU as competitor allowed
358 us to create the first map of targeted regions. We considered several caveats (polyspecificity of plasma
359 samples, absence of quaternary epitopes). We also carefully considered the possible nonspecific effect
360 of mutations on protein folding, which could generate misleading results. Certain mutants were,
361 indeed, poorly expressed and could not be used (Supplementary Table 3). A number of these limitations
362 may be overcome in the future with the use of alternative tools, such as human monoclonal antibodies
363 and subviral particles.

364 Human infection with zoonotic SFV represents a model for cross-species transmission of retroviruses
365 leading to persistent infection that is successfully controlled by the immune system. We have
366 previously reported the presence of potent nAbs in most infected individuals [20]. Here, we have
367 mapped major antigenic sites. Concerning the control of SFV in humans, a notable result from the
368 present study is that two immune escape mechanisms, sequence variation and glycan shielding, were
369 observed. The SFV RBD is structurally different from known and modelled retroviral RBDs [39]. We
370 have provided a novel model integrating structural, genetic, functional, and immunological knowledge
371 on the bimorphic SFV RBD. We have thus gained information on the two SFV genotypes that have
372 persisted for over 30 million years of evolution with their animal hosts. Through the study of SFV and
373 its unique properties, we should also gain fundamental knowledge on the structural basis for the
374 inhibition of viruses by nAbs.

375 Methods

376 Human plasma samples

377 Blood samples were drawn from adult populations living in villages and settlements throughout the
378 rainforests of Cameroon. Participants gave written informed consent. Ethics approval was obtained
379 from the relevant national authorities in Cameroon (the Ministry of Health and the National Ethics
380 Committee) and France (Commission Nationale de l'Informatique et des Libertés, Comité de Protection
381 des Personnes Ile de France IV). The study was registered at www.clinicaltrials.gov,
382 https://clinicaltrials.gov/ct2/show/NCT03225794/. SFV infection was diagnosed by a clearly positive
383 Gag doublet on Western blots using plasma samples from the participants and the amplification of the
384 integrase gene and/or LTR DNA fragments by PCR using cellular DNA isolated from blood buffy-coats
385 [3]. We identified the SFV origin by phylogenetic analysis of the integrase gene sequence [3]. The SFV

386 genotype was determined by amplification of the SUvar DNA fragment by PCR [7]. Plasma samples
387 from 24 participants were used for this study (Supplementary Tables 1 and 4). Four participants were not
388 infected with SFV and 20 were infected with a gorilla SFV.

389 Viral strains, amino-acid numbering, and Env domain nomenclature

390 We used sequences from primary zoonotic gorilla SFVs, SFVggo_huBAD468 (GI-D468, JQ867465) and
391 SFVggo_huBAK74 (GII-K74, JQ867464) [40] and the laboratory-adapted chimpanzee SFV,
392 SFVpsc_huPFV (CI-PFV, KX087159) [41] for the synthesis of foamy viral vectors (FVV) and envelope
393 proteins and peptides. For simple reference to previously described Env sequences and functions, we
394 used the amino-acid positions from the CI-PFV strain, unless otherwise stated. The GI-D468, GII-K74,
395 and CI-PFV sequence alignment are shown in supplementary Fig. 1. When referring to infecting SFV
396 strains and the antibodies raised against them, gorilla and chimpanzee genotype I SFV are referred to
397 as GI and CI, respectively; gorilla genotype II SFV is referred to as GII.

398 Cells

399 Baby hamster kidney (BHK)-21 cells (ATCC-CLL-10, hamster kidney fibroblast) were cultured in DMEM-
400 5% fetal bovine serum (FBS). HT1080 cells (ECACC 85111505, human fibrosarcoma) were cultured in
401 Eagle's Minimum Essential Medium with Earle's Balanced Salts and L-glutamine supplemented with
402 10% FBS and 1% L-glutamine. Human embryonic kidney 293T cells (Cat. N˚ 12022001, Sigma) were
403 cultured in DMEM-10% FBS. FreeStyle 293-F cells (Life Technologies) were cultured in Ex-cell 293 HEK
404 serum-free medium supplemented with 5 µg/mL phenol red sodium salt, 2% L-glutamine, and 0.2x
405 penicillin-streptomycin.

406 Peptides

407 At the beginning of the project, the SUvar (aa 248-488) sequences from the GI-D468 and GII-K74 strains
408 were analyzed using linear B-cell epitope prediction software available on the Immune Epitope Data
409 Base (http://tools.iedb.org/bcell/), which are based on known B-cell epitopes (LBtope [42]),
410 hydrophilicity (Parker prediction replaced by Bepipred software [43]), and protrusion outside of
411 globular proteins (Ellipro [44]). In addition, we manually inspected viral sequences for stretches of
412 genotype-specific epitopes. We selected 14 sequences and tested the corresponding GI-D468 and GII-
413 K74 peptides, as well as nine CI-PFV peptides from a previously synthesized peptide set [20]
414 (Supplementary Table 2). After resolution of the RBD crystal structure, we designed a novel peptide set
415 corresponding to the four loops located in the RBD upper subdomain [14]. As positive controls, we
416 used the N_{96}-V_{110} (NKDIQVLGPVIDWNV from SFV Env LP) and I_{176}-I_{199} (INTEPSQLPPTAPPLLPHSNLDHI
417 from HTLV-1 gp46) peptides containing immunodominant epitopes [20]. Peptides were synthesized by

418 Smartox SAS (Saint-Martin d'Hères, France) or Genscript (Leiden, The Netherlands) and were tested
419 individually.

420 ELISA

421 The protocol was described in [20]. Briefly, peptides diluted in carbonate buffer at 1 µg/mL were
422 coated on clear high-binding polystyrene 96-well microplates (Biotechne) overnight (ON) at +4°C.
423 Plasma samples were diluted at 1:200 in phosphate buffered saline (PBS)-0.1% bovine serum albumin
424 (BSA)-0.1% Tween20. Bound plasma antibodies were detected with horseradish peroxidase (HRP)-
425 conjugated goat anti-human IgG H+L (0.02 µg/mL, #109-035-008, Jackson Immuno Research Europe).
426 The peptide diluent was used as the negative control and antibody binding to peptides is expressed as
427 the difference in OD (Δ_{OD} = ODtest – ODcontrol). Plasma samples from three SFV-uninfected individuals
428 were tested for binding to the 37 peptides. The mean + 2 SD of Δ_{OD} (0.14) was used to define the
429 positivity cutoff. The proportion of responding individuals was calculated among those infected with a
430 given virus (SFV, n = 17; HTLV-1, n = 7).

431 Plasmids

432 The four-component CI-PFV FVV system (pcoPG, pcoPP, pcoPE, and pcu2MD9) and the gorilla SFV Env
433 constructs containing sequence from the zoonotic GI-D468 and GII-K74 *env* genes have already been
434 described [7, 45]. Novel plasmids were synthesized by Genscript (Piscataway, NJ, USA). We built a FVV
435 expressing β-galactosidase with a nuclear localization signal (puc2MD9-B-GAL) by replacement of the
436 *gfp* gene in the puc2MD9 backbone for easier image analysis on our quantification device. CI-PFV Env
437 deleted of RBDj or L3, GII-K74 Env deleted of RBDj or L2 or L4 were constructed with the boundaries
438 used for immunoadhesins (Supplementary Table 3).

439 Immunoadhesin constructs express a fusion protein formed by the murine IgK signal peptide, SFV SU
440 with deleted furin cleavage site (aa 127-567), and the heavy chain (hinge-CH2-CH3) of murine IgG2a.
441 A Twin-Strep-tag was fused after the mIgG2a to facilitate immunoadhesin purification, except for the
442 first immunoadhesin constructs (^{GII}ΔRBDj, ^{GII}swapRBDj and ^{GII}ΔN10). The murine leukemia virus (MLV)
443 gp70 SU (aa 34-475, strain FB29, NP_040334.1) was fused to the Twin-Strep-tag. All genes were codon
444 optimized for expression in mammalian cells and placed under the control of a CMV promotor and
445 intron in the pcZI plasmid [46].

446 The codon-optimized synthetic genes encoding GII-K74 SU (aa 127-566) and ectodomain (aa 91-907)
447 were cloned into the already described pT350 plasmid [47], which contains the *Drosophila*
448 metallothionein promoter, which is inducible by divalent cations [48], the *Drosophila* BiP signal peptide
449 (MKLCILLAVVAFVGLSLG) at the N-terminus and a Twin-Strep-tag
450 (AGWSHPQFEKGGGSGGGSGGGSWSHPQFEK) for affinity purification at the C-terminus. Stable S2 cell

451 lines were generated by antibiotic resistance and protein production was induced by the addition of 2
452 µM $CaCl_2$. For expression in mammalian cells, the murine IgK signal peptide was fused at the N-
453 terminus of codon-optimized genes encoding GII-K74 SU (aa 127-566). The genes were placed under
454 the control of the CMV promoter and intron [46] by insertion into the pcDNA3.1 vector.

455 ## Protein expression and purification

456 293-F cells were seeded at 2.5 10^6 cells/mL in FreeStyle 293 Expression medium and transfected by the
457 addition of plasmid DNA (2 µg/mL) and LipoD293 (6 µg/mL #SL100668, Tebu-bio). After 24 h, cells were
458 diluted 1:1 in Ex-cell culture media and cultivated for another 48 h and the supernatants collected and
459 stored at -80°C. For the expression of immunoadhesins with high-mannose-type glycans, transfected
460 cells were cultivated in the presence of 5 µM Kifunensine mannosidase inhibitor (#BML-S114-0005,
461 Enzo Life Sciences). Glycans were removed by incubating the immunoadhesins ON at room
462 temperature (RT) with endoglycosidase H (endo-H, 0.8 U/mL, #P0702L, New England Biolabs) in 50
463 mM Na acetate-50 mM NaCl, pH 6. Supernatants were thawed and filtrated through a 0.2 µm filter
464 before centrifugation at 4500 x g at 4°C in VivaSpin tubes (Sartorius). The first-generation
465 immunoadhesins do not carry the Twin-Strep-tag and were purified using Protein A Mag Sepharose™
466 Xtra beads (50 µL beads/mL of supernatant; #28-9670-62, GE Healthcare) using binding Buffer pH 7,
467 0.2 M Na_3PO_4 (#28-9030-59, Ab Buffer Kit, GE Healthcare). Beads were incubated at 4°C on a rotator
468 ON. Proteins were eluted with a pH 2.5 elution buffer containing 0.2 M Glycine-HCl and neutralized
469 with 1 M Tris-HCl, pH 9 (#PUR004, NEO Biotech, CliniSciencesProteus). Immunoadhesins and ^{MLV}SU
470 fused to Twin-Strep-tag were purified using Gravity Flow Strep-Tactin XT Superflow High-Capacity
471 columns (#2-4031-001, Iba Lifescience). Concentrated proteins were resuspended in buffer W at pH 8
472 and incubated with BioLock (#2-0205-050, Iba Life sciences) for 15 min at RT to neutralize biotin.
473 Loading onto the columns and elution were performed according to manufacturer's instructions.

474 GII-K74 SU, WT, and mutated ectodomains were expressed in *Drosophila* Schneider's cell line 2 (S2)
475 cells following the standard protocol [49]. GII monomeric SU and trimeric ectodomain proteins were
476 purified by affinity chromatography on a Streptactin column (IBA Biosciences), followed by size-
477 exclusion chromatography on Superdex 200, using standard methods provided by the manufacturers.

478 Protein concentrations were measured by NanoDrop. To verify protein purity and aggregate
479 formation, 1.5 µg of purified proteins was heat-denaturated at 70°C for 10 min in NuPAGE LDS sample
480 buffer (#NP0007, Introgen), with or without NuPAGE reducing buffer (50 mM DTT; #NP0009,
481 Invitrogen). Samples were loaded onto a precast NuPAGE 4-12% Bis-Tris gel (#NP0322, Invitrogen). The
482 gel was incubated with Bio-Safe Coomassie staining solution (#1610786, Bio-Rad) for 2 h with gentle
483 shaking, rinsed in H_2O ON, and imaged using a G:BOX (Syngene) (Supplementary Fig. 4).

484 ## Western blots

485 Western-blot analysis of protein expression was performed on cell supernatants. Samples were heat-
486 denaturated and reduced as described for purified proteins before loading onto precast NuPAGE 4-
487 12% Bis-Tris gels (#NP0322, Invitrogen). Proteins were migrated for 2-3 h at 120 V in NuPAGE MOPS
488 SDS running buffer (#NP0001, Invitrogen) and transferred onto a PVDF membrane (#1704156, Bio-Rad)
489 using a Trans-Blot Turbo transfer system (Bio-Rad). Membranes were blocked and antibody labeled in
490 Tris-buffered saline (TBS)-0.1%Tween-5% BSA. For Strep-tag detection, membranes were incubated
491 with StrepMAB-Classic monoclonal antibody conjugated to HRP (0.05 µg/mL, #2-1509-001, Iba
492 Lifesciences) for 2 h at RT. For SFV SU detection, membranes were incubated with a biotinylated anti-
493 SU murine antibody ON at 4°C (3E10, 1 µg/mL), washed three times in TBS-0.1% Tween for 10 min and
494 incubated with Streptavidin-HRP (1:2000, #DY998, Biotechne). Membranes were washed three times
495 in TBS-0.1% Tween for 10 min before revelation with SuperSignal West Pico PLUS chemiluminescence
496 substrate (#34579, ThermoFischer Scientific) and signal acquisition using a G:BOX.

497 ## Foamy viral vectors (FVVs)

498 FVV particles were produced by co-transfection of HEK293T cells by the four plasmids. Fifteen µg total
499 DNA (gag:env:pol:transgene ratio of 8:2:3:32) and 45 µl polyethyleneimine (#101-10N, JetPEI,
500 Polyplus) were added to a 10 cm^2 culture dish seeded with 4 x 10^6 293T cells. Supernatants were
501 collected 48 h post-transfection, clarified at 500 x g for 10 min, filtered using a 0.45 µm filter, and
502 stored as single-use aliquots at -80°C. FVVs were titrated as described [7, 50], with minor modifications
503 to optimize X-Gal staining of transduced cells, which was lighter than that of infected cells. Briefly, FVV
504 samples were thawed and clarified by spinning at 10,000 x g at 4°C for 10 min. Serial five-fold dilutions
505 were added in triplicate to sub-confluent BHK-21 cells seeded in 96-well plates and cultured for 72 h
506 at 37°C. Plates were fixed with 0.5% glutaraldehyde in PBS for 10 min at RT, washed with PBS, and
507 stained with 150 µl X-gal solution containing 2 mM $MgCl_2$, 10 mM potassium ferricyanide, 10 mM
508 potassium ferrocyanide, and 0.8 mg/mL 5-bromo-4-chloro-3-indolyl-B-D-galactopyranoside in PBS for
509 3 h at 37°C. Blue-stained cells were counted using an S6 Ultimate Image UV analyzer (CTL Europe,
510 Bonn, Germany). One infectious unit was defined as one blue cell. Cell transduction by FVV is a
511 surrogate for viral infectivity and FVV titers are expressed as infectious units (IU)/mL.

512 ## Neutralization assays

513 Prior to use in neutralization assays, plasma samples were diluted 1:10 in DMEM + 1 mM $MgCl_2$,
514 decomplemented by heating at 56°C for 30 min, and frozen at -80°C as single-use aliquots. Thawed
515 plasma samples were clarified by spinning at 10,000 x g for 10 min at 4°C. Serial two-fold dilutions were
516 incubated with FVV for 1 h at 37°C before titration in triplicate and residual infectivity quantified using

517 the 96-well plate microtitration assay described above. P96-well plates seeded with 5,000 BHK-21 cells
518 were exposed to 300 IUs of FVV. Plasma samples were initially titrated against replicating virus [7]. We
519 selected those with neutralization titers > 1:100 against the virus and performed plasma titration
520 against the FVV. We defined the plasma dilution required for a 90% reduction of FVV infectivity and
521 used it as the fixed concentration for the nAbs. Plasma samples were incubated with serial dilutions of
522 recombinant Env proteins for 1 h at 37°C. FVV was then mixed with the plasma/protein preparation
523 and incubated 1 h at 37°C before addition to BHK-21 cells. FVV infectivity was quantified 72 h later as
524 described for their titration. All conditions were tested in triplicate and the mean IU/well calculated.
525 Cells transduced with mock treated FVV (i.e., incubated with ^{MLV}SU at 20 nM or with medium) were
526 quantified on each plate and this value used as a reference. Relative infectivity was calculated for wells
527 treated with the plasma/protein mix and is expressed as the percentage of the reference value. The
528 WT immunoadhesin (^{GII}SU or ^{CI}SU) matched with the FVV Env was titrated along with the tested mutant
529 immunoadhesins on every plate in every experiment for each plasma tested. All immunoadhesins were
530 tested against each plasma at least twice and against at least four plasma samples. In the first assay
531 (screening), immunoadhesins were added at three concentrations, ranging from 200 to 2 nM. In the
532 second assay (confirmation), immunoadhesins with activity similar to that of WT or with no activity
533 were tested a second time at three dilutions. Mutant immunoadhesins with intermediate activity were
534 titrated in a three-fold serial dilution setting starting at 60 nM. We used two parameters to define the
535 action of the immunoadhesins on the nAbs from each plasma sample: maximum infectivity (MaxI) and
536 50% inhibitory concentration (IC_{50}). MaxI corresponds to the maximal infectivity in the presence of
537 immunoadhesin-blocking nAb and is defined as the mean relative infectivity at the two highest doses
538 tested. The IC_{50} values were calculated by plotting the relative infectivity as a function of
539 immunoadhesin concentration and a four parameters regression modeling of the Prism software
540 (Version 9, GraphPad). Mutant immunoadhesins with nAb activity similar to the WT one were given its
541 IC_{50}, and those with minimal or no activity were given an arbitrary IC_{50} value of 200 nM, corresponding
542 to the highest concentration of immunoadhesin tested.

543 SFV Env binding to cells

544 Immunoadhesins were thawed at RT and clarified at 10,000 x g for 10 min. HT1080 cells were treated
545 with trypsin-EDTA and 5 x 10^5 cells resuspended in 0.1 mL FACS buffer (PBS-0.1% BSA) containing the
546 immunoadhesins and incubated on ice for 1 h. Cells were washed twice and incubated with donkey
547 anti-murine IgG-(H+L)-AF488 (20 µg/mL, #A21202, Invitrogen) on ice for 30 min. Cells were washed
548 and resuspended in 0.2 mL PBS-2% PFA. Data were acquired on a CytoFlex cytometer (Beckman
549 Coulter) and analyzed using Kaluza software. A minimum of 25,000 cells were acquired. Single cells
550 were selected by sequential gating on FSC-A/SSC-A and SSC-A/SSC-H dot-plots (Supplementary Fig. 8).

551 Immunoadhesin binding is expressed as the ratio of mean fluorescence intensity (MFI) of
552 immunoadhesin-treated over untreated cells. Each immunoadhesin was tested twice at 3, 30, and 300
553 nM. The MFI ratios were plotted as a function of immunoadhesin concentration and the area under
554 the curve was calculated (Supplementary Fig. 5). To limit inter-experimental variation, WT
555 immunoadhesins were included in every experiment and the binding level of mutant immunoadhesins
556 normalized to that of the WT.

557 Analysis of FVVs carrying mutated Env

558 The yield of FVV particles was estimated by quantifying particle-associated transgene RNA. FVV RNA
559 was extracted from raw cell supernatants using a QIAamp Viral RNA Extraction Kit (Qiagen), treated
560 with a DNA-free kit (Life Technologies), and retro-transcribed with Maxima H Minus Reverse
561 Transcriptase (Thermo Fischer Scientific) using random primers (Thermo Fischer Scientific) according
562 to the manufacturers' instructions. qPCR was performed on cDNA using BGAL primers (BGAL_F 5'
563 AAACTCGCAAGCCGACTGAT 3' and BGAL_R 5' ATATCGCGGCTCAGTTCGAG 3') with a 10-min
564 denaturation step at 95°C and 40 amplification cycles (15 s at 95°C, 20 s at 60°C, and 30 s at 72°C)
565 carried out using an Eppendorf realplex2 Mastercycler (Eppendorf). A standard curve prepared with
566 serial dilutions of pcu2MD9-BGAL plasmid was used to determine the FVV copy number. Results are
567 expressed as vector particles/mL, considering that each particle carries two copies of the transgene.

568 The expression level of mutated Env proteins in producer cells was assessed by western-blot analysis.
569 293T cells transfected to produce FVVs were collected and lysed in RIPA buffer (#R0278, Sigma)
570 containing protease inhibitors (#11140920, Roche) for 2 h at 4°C. Samples were heat-denaturated at
571 70°C for 10 min in LDS sample buffer (NuPage) and 50 mM DTT before loading onto a precast NuPAGE
572 4-12% Bis-Tris gel (Invitrogen) and migration for 2 h at 120 V in MOPS running buffer. The content of
573 ≈ one million cells was analyzed. Samples were transferred onto a PVDF membrane using a Trans-Blot
574 Turbo transfer system (Bio-Rad, Hercules, CA, USA). Membrane blockade and antibody labelling were
575 performed in TBS-0.1%Tween-5%BSA. Membranes were incubated with an anti-LP antibody ON at 4°C
576 (clone P6G11-G11, 1 µg/mL), washed, and incubated with a goat anti-mouse secondary antibody HRP
577 conjugate (1:10000, #31430, Invitrogen). Membranes were washed three times in TBS-0.1% Tween for
578 10 min before revelation using Immobilon ECL Ultra Western HRP Substrate (WBULS0100, Merck) and
579 signal acquisition on an Amersham Imager 680 (GE Healthcare).

580 To test the capacity of mutated Env to mediate the binding of vector particles to cells, HT1080 cells
581 were incubated with the FVV particles (1, 10 and 100 particles/cell) on ice for 1 h. The cells were
582 washed three times with PBS to eliminate unbound FVV and RNA was extracted using an RNeasy plus
583 mini-Kit (Qiagen) according to manufacturer's protocol and RT performed as described for FVV RNA

584 quantification. Bound FVV was quantified by qPCR of the *bgal* gene as described for vector titration;
585 cells were quantified by qPCR amplification of the *hgapdh* gene with the following primers: hGAPDH_F
586 5' GGAGCGAGATCCCTCCAAAAT 3' and hGAPDH_R 5' GGCTGTTGTCATACTTCTCATGG 3'. The qPCR
587 reaction conditions were the same as those used to amplify the *bgal* gene. The relative mRNA
588 expression of *bgal* versus *hgapdh* was calculated using the -ΔΔCt method, and relative binding as 2-
589 ΔΔCt.

590 ### Statistical analysis

591 Mutations in the immunoadhesins modified their ability to block the nAbs in two ways: either by
592 reducing avidity, leading to a higher IC_{50}, or by the fraction of plasma nAb blocked, leading to lower
593 maximal infectivity. For each plasma sample, the IC_{50} and MaxI were tested for the WT immunoadhesin
594 in at least five experiments. The threshold value defining a statistically significant change rerlative to
595 WT was defined as the mean + 3*SD for the IC_{50} and the mean - 3*SD for MaxI. Thresholds were defined
596 for each plasma sample. The infectious titers, particle concentration, percentage of infectious
597 particles, and quantity of bound FVV carrying WT and mutant immunoadhesins were compared using
598 the ANOVA test for paired samples and Sidak's multiple comparisons test (GraphPad Prism 9 software).

599 ## Acknowledgements

600 We thank H. Mouquet and V. Lorin for sharing the 293-F cells and advice. We are grateful to Mathilde
601 Couteaudier for mentoring MD and LTD in their performance of the experimental work. We used
602 devices from the Cytometry and Biomarker Utechs at the Institut Pasteur and we thank their staff for
603 their support and advice. We thank Delphine Brun from the Unité de Virologie Structurale for technical
604 assistance. The manuscript has been edited by a native English speaker.

605 ## Funding

606 This work was supported by the Agence Nationale de la Recherche (ANR-10-LABX62-IBEID, Intra-Labex
607 Grant (M.B.)), and the Programme de Recherche Transversal from the Institut Pasteur (PTR2020-353
608 ZOOFOAMENV, F.B.). SFV protein production was supported by the European Virus Archive-GLOBAL
609 project, which has received funding from the EU Horizon 2020 Research and Innovation Programme
610 (grant agreement number 871029). L.T.D. was supported by the Pasteur-Paris-University (PPU)
611 International Doctoral Program and the Fondation pour la Recherche Médicale, including additional
612 supportive funding from the Danish Pasteur Society, Augustinus Fonden, Knud-Højgaards Fond, and
613 Viet-Jacobsen Fonden. The funding agencies had no role in the study design, generation of results, or
614 writing of the manuscript.

615 ## Authors contribution

616 FB, MB, FR, and AG designed the project. FB and MB supervised the project and acquired funding. LTD,
617 IF, YC, MD, and TM performed the experiments. LTD, IF, FB, and MB analyzed the data. AG, RN, and
618 CBN collected the human samples. LTD and YC provided figures and text elements for the draft. FB
619 wrote the initial and final drafts. All authors participated in reviewing the drafts.

620 ## References

621 1. Rethwilm, A. and J. Bodem, Evolution of foamy viruses: the most ancient of all retroviruses.
622 *Viruses* **5,** 2349-2374 (2013).
623 2. Pinto-Santini, D.M., C.R. Stenbak, and M.L. Linial, Foamy virus zoonotic infections.
624 *Retrovirology* **14,** 55 (2017).
625 3. Betsem, E., R. Rua, P. Tortevoye, A. Froment, and A. Gessain, Frequent and recent human
626 acquisition of simian foamy viruses through apes' bites in Central Africa. *PLoS Pathog.* **7,**
627 e1002306 (2011).
628 4. Filippone, C., et al., A severe bite from a nonhuman primate is a major risk factor for HTLV-1
629 infection in hunters from Central Africa. *Clin. Infect. Dis.* **60,** 1667-1676 (2015).
630 5. Buseyne, F., et al., Clinical signs and blood test results among humans infected with zoonotic
631 simian foamy virus: a case-control study. *J. Infect. Dis.* **218,** 144-151 (2018).
632 6. Gessain, A., et al., Case-control study of immune status in humans infected with zoonotic
633 gorilla simian foamy viruses. *J. Infect. Dis.* **221,** 1724-1733 (2020).
634 7. Lambert, C., et al., Potent neutralizing antibodies in humans infected with zoonotic simian
635 foamy viruses target conserved epitopes located in the dimorphic domain of the surface
636 envelope protein. *PLoS Pathog.* **14,** e1007293 (2018).
637 8. Williams, D.K. and A.S. Khan, Role of neutralizing antibodies in controlling simian foamy virus
638 transmission and infection. *Transfusion* **50,** 200-207 (2010).
639 9. Couteaudier, M., et al., Plasma antibodies from humans infected with zoonotic simian foamy
640 virus do not inhibit cell-to-cell transmission of the virus despite binding to the surface of
641 infected cells. *PLoS Pathog.* **18,** e1010470 (2022).
642 10. Galvin, T.A., I.A. Ahmed, M. Shahabuddin, T. Bryan, and A.S. Khan, Identification of
643 recombination in the envelope gene of simian foamy virus serotype 2 isolated from Macaca
644 cyclopis. *J. Virol.* **87,** 8792-8797 (2013).
645 11. Richard, L., et al., Cocirculation of two *env* molecular variants, of possible recombinant origin,
646 in gorilla and chimpanzee simian foamy virus strains from Central Africa. *J. Virol.* **89,** 12480-
647 12491 (2015).
648 12. Aiewsakun, P., et al., Modular nature of simian foamy virus genomes and their evolutionary
649 history. *Virus Evol.* **5,** vez032 (2019).
650 13. Duda, A., D. Luftenegger, T. Pietschmann, and D. Lindemann, Characterization of the prototype
651 foamy virus envelope glycoprotein receptor-binding domain. *J. Virol.* **80,** 8158-8167 (2006).
652 14. Fernandez, I., et al., The crystal structure of a simian Foamy Virus receptor binding domain
653 provides clues on the entry to host cells. (2022, submitted).
654 15. Couteaudier, M., D. Calzada-Fraile, T. Montange, A. Gessain, and F. Buseyne, Inhibitors of the
655 interferon response increase the replication of gorilla simian foamy viruses. *Virology* **541,** 25-
656 31 (2020).
657 16. Rua, R., E. Betsem, T. Montange, F. Buseyne, and A. Gessain, *In vivo* cellular tropism of gorilla
658 simian foamy virus in blood of infected humans. *J. Virol.* **88,** 13429-13435 (2014).
659 17. Luftenegger, D., M. Picard-Maureau, N. Stanke, A. Rethwilm, and D. Lindemann, Analysis and
660 function of prototype foamy virus envelope N glycosylation. *J. Virol.* **79,** 7664-7672 (2005).

661 18. Berg, A., T. Pietschmann, A. Rethwilm, and D. Lindemann, Determinants of foamy virus
662 envelope glycoprotein mediated resistance to superinfection. *Virology* **314,** 243-252 (2003).
663 19. Effantin, G., et al., Cryo-electron microscopy structure of the native prototype foamy virus
664 glycoprotein and virus architecture. *PLoS Pathog.* **12,** e1005721 (2016).
665 20. Lambert, C., et al., An immunodominant and conserved B-cell epitope in the envelope of
666 simian foamy virus recognized by humans infected with zoonotic strains from apes. *J. Virol.* **93,**
667 e00068-00019 (2019).
668 21. Netzer, K.O., A. Rethwilm, B. Maurer, and V. Termeulen, Identification of the major
669 immunogenic structural proteins of human foamy virus. *J. Gen. Virol.* **71,** 1237-1241 (1990).
670 22. Hahn, H., et al., Reactivity of primate sera to foamy virus Gag and Bet proteins. *J. Gen. Virol.*
671 **75,** 2635-2644 (1994).
672 23. Herchenroder, O., et al., Specific binding of recombinant foamy virus envelope protein to host
673 cells correlates with susceptibility to infection. *Virology* **255,** 228-236 (1999).
674 24. Cummins, J.E., et al., Mucosal and systemic antibody responses in humans infected with simian
675 foamy virus. *J. Virol.* **79,** 13186-13189 (2005).
676 25. Switzer, W.M., et al., Ancient co-speciation of simian foamy viruses and primates. *Nature* **434,**
677 376-380 (2005).
678 26. McCoy, L.E., et al., Incomplete neutralization and deviation from sigmoidal neutralization
679 curves for HIV broadly neutralizing monoclonal antibodies. *PLoS Pathog.* **11,** e1005110 (2015).
680 27. Doores, K.J. and D.R. Burton, Variable loop glycan dependency of the broad and potent HIV-1-
681 neutralizing antibodies PG9 and PG16. *J. Virol.* **84,** 10510-10521 (2010).
682 28. Kim, A.S., D.P. Leaman, and M.B. Zwick, Antibody to gp41 MPER alters functional properties of
683 HIV-1 Env without complete neutralization. *PLoS Pathog.* **10,** e1004271 (2014).
684 29. Prasad, V.M., et al., Cryo-ET of Env on intact HIV virions reveals structural variation and
685 positioning on the Gag lattice. *Cell* **185,** 641-653 (2022).
686 30. Hill, C.L., P.D. Bieniasz, and M.O. McClure, Properties of human foamy virus relevant to its
687 development as a vector for gene therapy. *J. Gen. Virol.* **80,** 2003-2009 (1999).
688 31. Burkhart, M.D., S.C. Kayman, Y.X. He, and A. Pinter, Distinct mechanisms of neutralization by
689 monoclonal antibodies specific for sites in the N-terminal or C-terminal domain of murine
690 leukemia virus SU. *J. Virol.* **77,** 3993-4003 (2003).
691 32. Chuang, G.Y., et al., Structural Survey of Broadly Neutralizing Antibodies Targeting the HIV-1
692 Env Trimer Delineates Epitope Categories and Characteristics of Recognition. *Structure* **27,**
693 196-206.e196 (2019).
694 33. Murin, C.D., I.A. Wilson, and A.B. Ward, Antibody responses to viral infections: a structural
695 perspective across three different enveloped viruses. *Nature Microbiology* **4,** 734-747 (2019).
696 34. McLellan, J.S., et al., Structure of HIV-1 gp120 V1/V2 domain with broadly neutralizing
697 antibody PG9. *Nature* **480,** 336-U386 (2011).
698 35. Milligan, J.C., et al., Asymmetric and non-stoichiometric glycoprotein recognition by two
699 distinct antibodies results in broad protection against ebolaviruses. *Cell* **185,** 995-1007.e1018
700 (2022).
701 36. Bangaru, S., et al., A site of vulnerability on the Influenza virus hemagglutinin head domain
702 trimer interface. *Cell* **177,** 1136-1152.e1118 (2019).
703 37. Turner, H.L., et al., Disassembly of HIV envelope glycoprotein trimer immunogens is driven by
704 antibodies elicited via immunization. *Science Adv.* **7,** eabh2791 (2021).
705 38. Bermejo-Jambrina, M., et al., Infection and transmission of SARS-CoV-2 depend on heparan
706 sulfate proteoglycans. *EMBO J.* **40,** e106765 (2021).
707 39. Hötzel, I., Deep-time structural evolution of retroviral and filoviral surface envelope proteins.
708 *J. Virol.* **96,** e00063-00022 (2022).
709 40. Rua, R., E. Betsem, S. Calattini, A. Saib, and A. Gessain, Genetic characterization of simian
710 foamy viruses infecting humans. *J. Virol.* **86,** 13350-13359 (2012).
711 41. Wagner, T.C. and J. Bodem, Sequence errors in foamy virus sequences in the GenBank
712 database: resequencing of the prototypic foamy virus proviral plasmids. *Arch. Virol.* (2016).

713 42. Singh, H., H.R. Ansari, and G.P. Raghava, Improved method for linear B-cell epitope prediction
714 using antigen's primary sequence. *PLoS One* **8,** e62216 (2013).
715 43. Larsen, J.E., O. Lund, and M. Nielsen, Improved method for predicting linear B-cell epitopes.
716 *Immunome Res.* **2,** 2 (2006).
717 44. Ponomarenko, J., et al., ElliPro: a new structure-based tool for the prediction of antibody
718 epitopes. *BMC Bioinformatics* **9,** 514 (2008).
719 45. Hutter, S., E. Mullers, N. Stanke, J. Reh, and D. Lindemann, Prototype foamy virus protease
720 activity is essential for intraparticle reverse transcription initiation but not absolutely required
721 for uncoating upon host cell entry. *J. Virol.* **87,** 3163-3176 (2013).
722 46. Heinkelein, M., et al., Improved primate foamy virus vectors and packaging constructs. *J. Virol.*
723 **76,** 3774-3783 (2002).
724 47. Krey, T., et al., The disulfide bonds in glycoprotein E2 of hepatitis C virus reveal the tertiary
725 organization of the molecule. *PLoS Pathog.* **6,** e1000762 (2010).
726 48. Bunch, T.A., Y. Grinblat, and L.S. Goldstein, Characterization and use of the Drosophila
727 metallothionein promoter in cultured Drosophila melanogaster cells. *Nucl. Acids Res.* **16,** 1043-
728 1061 (1988).
729 49. Backovic, M. and T. Krey, Stable drosophila cell lines: An alternative approach to exogenous
730 protein expression. *Meth. Mol. Biol.* **1350,** 349-358 (2016).
731 50. Lambert, C., R. Rua, A. Gessain, and F. Buseyne, A new sensitive indicator cell line reveals cross-
732 transactivation of the viral LTR by gorilla and chimpanzee simian foamy viruses. *Virology* **496,**
733 219-226 (2016).
734 51. Gliniak, B.C., S.L. Kozak, R.T. Jones, and D. Kabat, Disulfide bonding controls the processing of
735 retroviral envelope glycoproteins. *J Biol Chem* **266,** 22991-22997 (1991).
736 52. Kelley, L.A., S. Mezulis, C.M. Yates, M.N. Wass, and M.J. Sternberg, The Phyre2 web portal for
737 protein modeling, prediction and analysis. *Nat. Protoc.* **10,** 845-858 (2015).
738 53. Ansari, H.R. and G.P. Raghava, Identification of conformational B-cell Epitopes in an antigen
739 from its primary sequence. *Immunome Res.* **6,** 6 (2010).

740

741 # Figure legends

742 ## Figure 1. SFV Env

743 Schematic representation of SFV Env. The precursor Env protein is cleaved by furin-like protease(s) at
744 two sites (vertical bars) to generate LP, SU, and TM. The dark sections highlight the transmembrane
745 regions of LP (H) and TM (MSD), and the fusion peptide (F). The minimal continuous RBD (aa 225-555,
746 blue background) comprises two regions essential for SU binding to cells, RBD1 (aa 225-396) and RBD2
747 (aa 484-555) [13]. The intervening region (aa 397-483), named RBDj, can be deleted without abrogating
748 binding to susceptible cells. B.The genotype-specific variable SU region (SUvar, aa 248-488) partially
749 overlaps with the RBD and is the exclusive target of nAbs [7]. C. The structure of the GII-K74 RBD
750 monomer (aa 218-552, PDB code 8AEZ, [14]) is presented in cartoon with glycans shown as sticks.
751 RBD1, RBD2, and RBDj regions are color-coded as on panel A. Structural elements relevant for the
752 present study are indicated, and the full description of the structure is available in [14]. D. The SUvar
753 region (red) is rendered as solvent accessible surface. The conserved region (SUcon) is displayed in
754 cartoon. The dashed line indicates the boundary between the lower and upper RBD subdomains.

755 ## Figure 2. Only a small proportion of plasma samples bind to peptides covering the SUvar
756 domain

757 Seventeen plasma samples from African hunters were tested for binding to 37 peptides located in the
758 SUvar domain (Supplementary Table 2). The summary graph shows positive responses (Δ_{OD}, y-axis)
759 plotted against peptides identified by the position of their first aa (x-axis). Plasma samples are
760 identified by a color code corresponding to the genotype(s) of the infecting strains (blue: infected with
761 a GI strain, red: infected with a GII strain, purple: infected by strains of both genotypes [7]). Left,
762 peptides spanning GI SUvar; right, peptides spanning GII SUvar; the RBDj region is indicated by the
763 lighter color. Detailed binding activity is shown on the aligned SU sequences; the RBDj sequence is
764 highlighted in italic characters; the sequence covered by peptides is highlighted by grey background.
765 Recognized peptides are underscored and designated by the same letters as those used in panel A.
766 Reactive plasma samples are indicated above the sequence and colored according to the genotype(s)
767 of the infecting strains. Six plasma samples from SFV-infected individuals reacted against seven
768 peptides located in the RBDj region (BAD551, BAK55, BAK56, BAK74, BAK82, and BAK132) and two
769 samples reacted against a peptide located in the RBD1 or RBD2 subdomains (BAD468 and BAK56,
770 respectively). Plasma antibody binding to the peptides was not genotype-specific. For example, sample
771 BAK56 reacted against peptide b (399W-K418) from the GI-D468 and GII-K74 strains.

772 ## Figure 3. The SFV SU block nAbs without affecting viral entry

773 A. Schematic presentation of the neutralization assay using SU immunoadhesin as competitor. Plasma
774 samples were diluted to achieve a reduction in the number of FVV-transduced cells by 90%. WT
775 immunoadhesins compete with Env on FVV for binding by nAbs, resulting in a higher number of FVV-
776 transduced cells; mutations in SU that affect binding by nAbs result in inefficient competition and
777 reduced FVV transduction. Representative images of wells with FVV-transduced cells stained by X-gal
778 are shown. B. Schematic representation of titration curves corresponding to SU mutants that loose
779 their capacity to block a fraction of nAbs (mut1, green), block all nAbs with reduced affinity (mut2 SU,
780 orange), or block a fraction of nAbs with reduced affinity (mut 3, pink) or those with no blocking activity
781 (mut4, purple). The curves are summarized by two parameters, MaxI and IC_{50}, which were compared
782 to those obtained with WT SU (panel C and D) to define significant differences in binding (see Materials
783 and Methods). C. The BAK132 (anti-GI) and MEBAK88 (anti-GII) plasma samples were incubated with
784 immunoadhesins and the mix added to FVVs expressing matched Env before titration. The relative
785 proportion of transduced cells is expressed as the percentage of cells transduced by untreated FVVs
786 (no plasma and no protein), is referred to as the relative infectivity, and is presented as a function of
787 protein concentration. The addition of ^{CI}SU (blue symbols) inhibited the action of nAbs from sample
788 BAK132, as shown by increased CI-PFV Env FVV relative infectivity, whereas ^{GII}SU (red symbols) had no
789 effect. Conversely, ^{GII}SU inhibited the action of nAbs from sample MEBAK88. ^{MLV}SU (grey symbols) had
790 no effect on the plasma antibodies. D. The infectivity of the CI-PFV and GII-K74 Env vectors was
791 quantified in the presence of ^{CI}SU, ^{GII}SU, and ^{MLV}SU; the relative infectivity is presented as a function of
792 protein concentration. E and F. Thirteen pairs of plasma samples and genotype-matched
793 immunoadhesins were tested at least five times for their activity against FFVs. The mean and standard
794 error of the mean of the IC_{50} (panel E) and MaxI (panel F) are shown for the CI-PFV Env vectors and
795 anti-GI plasma samples (blue symbols) and the GII-K74 Env vectors and anti-GII plasma samples (red
796 symbols).

797 ## Figure 4. SFV-specific nAbs recognize glycans on SUvar

798 A. Schematic representation of N-glycosylation sites on the SUvar domain. The N7' site (position 374,
799 brown symbol) is absent from CI-PFV but present in zoonotic gorilla SFV and several chimpanzee SFVs
800 [11]. The N8 site (position 391, bold stem) is required for SU expression [17]. The N10 site has a
801 genotype-specific location (N411 in GII strains, red symbol; N422 or 423 in GI/CI strains, blue symbol).
802 The glycosylation sites outside SUvar are shown in grey. B. The RBD is shown as a solvent accessible
803 surface, with SUvar in dark grey and SUcon in light grey. Side chains of the glycans are shown in orange
804 and were identified on deglycosylated RBD; the N5 glycan was poorly resolved and N286 is colored to
805 indicate the localization of its anchor. C and D. To determine whether SFV-specific nAbs target residue

806 glycosylated epitopes, vectors carrying CI-PFV or GII-K74 Env were mixed with four genotype-matched
807 plasma samples previously incubated with untreated, kifunensine (C), or kifunensine and endo-H
808 treated (D) ^{GII}SU at several concentrations. E. To test whether nAbs target the genotype-specific N10
809 glycosylation site, the immunoadhesin in which N10 was inactivated (^{GII}ΔN10) was incubated with four
810 genotype-matched plasma samples. F. Residues 407-413 were swapped with those from the GI-D468
811 strain and the resulting ^{GII}swap407 was tested for its ability to block four anti-GII plasma samples. The
812 glycosylation sites located on the immunoadhesins were inactivated one by one (except N8) and tested
813 for their inability to block four GII-specific plasma samples (G to K). ^{GII}ΔN7' was tested against three
814 additional samples to confirm its impact on nAbs (J). For each plasma sample, the IC_{50} is presented as
815 a function of MaxI for untreated and enzyme-treated ^{GII}SU (C and D) or ^{GII}SU and mutated
816 immunoadhesins (E to K). The IC_{50} and MaxI values for untreated ^{GII}SU are presented as open symbols
817 and are from the same experiment in which the mutant immunoadhesins were tested. For the enzyme-
818 treated and mutated immunoadhesins, the symbols are colored according to the IC_{50} and MaxI
819 thresholds that were used to statistically define significant differences from ^{GII}SU.

820 Figure 5. Most SFV-specific nAbs recognize the RBDj domain

821 A. Schematic representation of functional RBD subdomains [13], loops, and HBS identified in [14]. B.
822 The RBD is shown as a solvent accessible surface with SUvar in dark grey, SUcon in light grey, L2 in
823 orange, L3 in green, L4 in maroon, and HBS in black. To locate SFV-specific nAb epitopes on SU
824 functional domains, vectors carrying GII-K74 Env were treated with GII-specific plasma samples
825 previously incubated with ^{GII}SU and mutant immunoadhesin with RDBj deleted (^{GII}ΔRBDj, C), the Env
826 ectodomain with WT or mutated HBS (^{GII}K342A-R343A in panel D and ^{GII}K356A-R369A in panel E), and
827 immunoadhesins with deleted loops (^{GII}ΔL2, ^{GII}ΔL3, and ^{GII}ΔL4 in panels F to H). For each plasma sample,
828 the IC_{50} is presented as a function of MaxI for ^{GII}SU and the mutated immunoadhesins. The IC_{50} and
829 MaxI values for ^{GII}SU are presented as open symbols and are from the same experiment in which the
830 mutant immunoadhesins were tested. Symbols are colored according to the IC_{50} and MaxI thresholds
831 used to define statistically significant differences from ^{GII}SU; we applied the same threshold values for
832 the analyses of the Env ectodomain, which had the same inhibitory activity as ^{GII}SU (Supplementary Fig.
833 2).

834 Figure 6. Epitope disruption by glycan insertion revealed additional sites recognized by
835 nAbs

836 A. Schematic representation of the seven sites of glycan insertion on SU. Functional RBD subdomains
837 and loops are indicated using the same color code as in Fig.5. B. The RBD is shown as a solvent
838 accessible surface with SUvar in dark grey, SUcon in light grey, and the seven glycan insertion sites in

839 orange; front (top) and back (bottom) views are shown. B'. The 345-353 loop and adjacent helix are
840 presented as ribbons and side chains for GII-K74 (red) and CI-PFV (blue, AlphaFold2-predicted
841 structure). C to I: Seven candidate genotype-specific sequences (Supplementary Table 5) were disrupted
842 by inserting glycans in the immunoadhesins that were tested for their capacity to block nAbs. J to M:
843 five mutant immunoadhesins were tested to characterize the epitopic region in the 345-353 loop. All
844 mutants were tested against at least four plasma samples. Those for which the capacity to block nAbs
845 was the most altered were then tested on additional samples. For each plasma sample, the IC_{50} is
846 presented as a function of MaxI for ^{GII}SU and the mutant SUs. The IC_{50} and MaxI values of ^{GII}SU are
847 presented as open symbols and are those from the same experiment in which the mutated
848 immunoadhesins were tested. Symbols are colored according to the IC_{50} and MaxI thresholds used to
849 statistically define significant differences from ^{GII}SU. ^{GII}swap333 was tested twice at three
850 concentrations and showed similar blocking capacity as ^{GII}SU; the IC_{50} values were arbitrarily set to the
851 same level as those of ^{GII}SU (see Materials and Methods).

852 ## Figure 7. GI and GII-specific nAbs target different epitopes

853 CI SU immunoadhesins with mutations matching the most informative GII-K74 mutations were tested
854 for their capacity to block nAbs from GI-specific plasma samples. A, Kifunensin-treated ^{CI}SU; B,
855 Kifunensin and endoH-treated ^{CI}SU; C, ^{CI}ΔN10; D, $^{CI}350_{glyc}$; E, ^{CI}ΔRBDj; F, ^{CI}ΔL2; G, ^{CI}ΔL3; H, ^{CI}ΔL4; I,
856 $^{CI}463_{glyc}$; J, ^{GII}swapRBDj; K, ^{GII}SU; L, ^{CI}swapL3. All mutants were tested against four plasma samples.
857 Those for which the capacity to block nAbs was the most altered were then tested on additional
858 samples. For each plasma sample, the IC_{50} is presented as a function of MaxI for the ^{CI}SU and mutant
859 immunoadhesins. The IC_{50} and MaxI values of ^{CI}SU are presented as open symbols and are those from
860 the same experiment in which the mutant immunoadhesins were tested. For mutant immunoadhesins,
861 the symbols are colored according to the IC_{50} and MaxI thresholds used to statistically define significant
862 differences from ^{CI}SU. The red lines correspond to data obtained with GII-specific plasma samples
863 against equivalent constructs (Panels 4C, 4D, 4E, 5C, 5F, 5H, 6E, and 6H match panels 7A to 7H,
864 respectively).

865 ## Figure 8. Most samples contain nAbs that recognize several epitopic regions on SUvar

866 The results from competition experiments were summarized for each plasma sample and for the
867 mutant immunoadhesins from the most targeted regions (apex, 345-353 loop, and the N7' region).
868 Four outcomes are presented: same recognition as WT SU (green), recognition with reduced affinity
869 (i.e., increased IC_{50}, orange vertical shading), blocking a smaller fraction of nAbs than WT SU (i.e.,
870 reduced MaxI, orange horizontal shading), or having both effects, orange. Black squares indicate the
871 major epitopic regions of the GII- and GI-specific samples (panels A and B, respectively). Within each

872 epitopic region defined by several mutant immunoadhesins, nAb specificity varied between
873 individuals.

874 Figure 9. nAbs target epitopic regions involved in SU binding to susceptible cells or
875 required for viral infectivity

876 A. HT1080 cells were incubated with the panel of tested immunadhesins (Fig. 4 to 7). Cell-bound
877 immunoadhesins were detected by staining with a fluorescently labeled antibody targeting the murine
878 IgG Fc fragment. Stained cells were analyzed on a flow cell cytometer. Supplementary Fig. 8 presents the
879 gating strategy and normalization of the results to the levels of bound WT immunoadhesins (^{GII}SU and
880 ^{CI}SU). Binding levels of GII mutants (red symbols) are presented in the same order as in Fig. 4, 5 and 6.
881 CI mutants (blue symbols) are presented side-by-side with the corresponding and related GII mutants,
882 with a colored background. Mutated HBS shows reduced binding to susceptible cells, as shown in [14].
883 C. Three batches of FVVs carrying WT or mutated Env were produced. The concentration of vector
884 particles was quantified by RT-qPCR amplification of the *bgal* transgene. Each batch was titrated twice
885 and the mean titers are presented; lines represent the mean values from the three FVV batches. D.
886 FVV infectious titers were quantified on BHK-21 cells. Each batch was titrated twice and the mean titers
887 are presented; lines represent the mean values from the three FVV batches. E. FVVs carrying WT and
888 mutated Env were incubated with HT1080 cells on ice for 1 h before washing and quantification of *bgal*
889 mRNA incorporated in the vector particles and the *gapdh* gene of susceptible cells. The FVV dose was
890 10 FVV particles per cell. The levels of *bgal* and cellular *gapdh* mRNA were quantified by RT-qPCR; the
891 ΔΔCt method was used to calculate the relative amount of FVV particles bound to cells. Values below
892 the threshold were arbitrarily set at 0.0005. Lines represent the mean values from tested FVV batches.
893 The dotted lines in panels B to D represent the quantification threshold. The infectious titers, particle
894 concentration, and levels of bound particles from FVVs carrying mutant or WT SU were compared using
895 the ANOVA test and Sidak's multiple comparison test, *$p < 0.05$, **$p < 0.01$, ***$p < 0.001$, ****$p <$
896 0.0001.

897

898 Figure 10. Schematic summary of current knowledge on SFV Env.

899 A. The RBD domain is composed of two subdomains located at the top of Env trimers; the drawing
900 highlights the region involved in trimer assembly and the HBS [14, 19]. B. Genetic studies on SFV strains
901 circulating in Central Africa have identified two genotypes that differ in the sequence encoding the
902 central part of the SU (SUvar) domain [11, 12]. The SUvar domain forms the upper part of the RBD
903 ($SUvar^{Up}$) prolonged, in the lower subdomain, by an arm ($SUvar^{Lo}$) wrapping around the stem of which
904 the sequence is conserved (SUcon). Binding studies defined the RBD as being bipartite, with two
905 essential binding regions (RBD1 and RBD2) separated by RBDj [13]. These regions form the bottom of
906 $SUvar^{Up}$ and $SUvar^{Lo}$ (variable part of RBD1), the top of $SUvar^{Up}$ (RBDj), and the stem (short conserved
907 fragment of RBD1 and RBD2). C. nAbs exclusively target the SUvar domain [7]. In the present paper,
908 we identified GII-specific epitopes in the $SUvar^{Up}$ and $SUvar^{Lo}$ domains and GI-specific epitopes in
909 $SUvar^{Up}$ only. nAbs recognized L2, L3, and L4 of $SUvar^{Up}$ and the N7' region and 345-353 loop of $SUvar^{Lo}$
910 (lines ending with a dot). Glycans inserted in both domains revealed additional epitopic sites (lines
911 ending with a triangle).

912

913

914 Figure 1. SFV Env

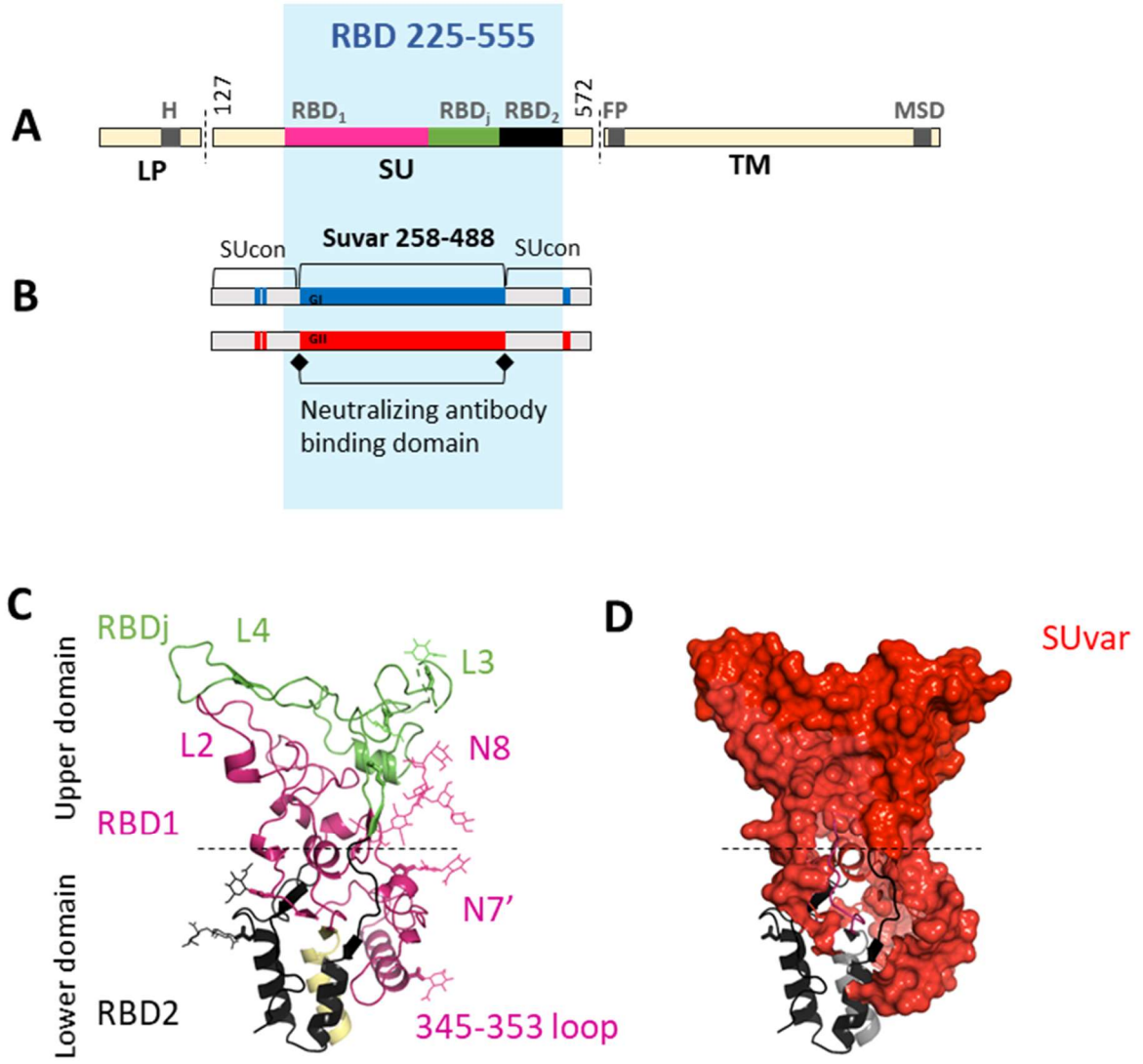

915

916

Figure 2. Only a small proportion of plasma samples bind to peptides spanning the SUvar domain

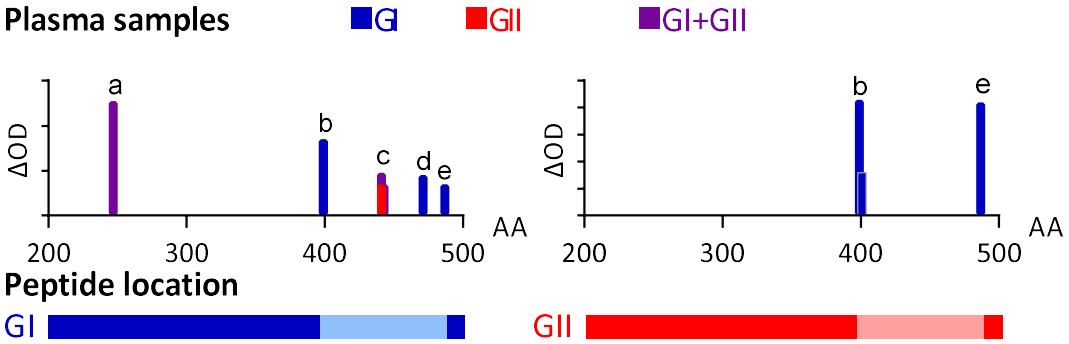


```
CI-PFV      LVKYKEPKPW PKEGLIADQC PLPGYHAGLT YNRQSIWDYY   276
                       BAD468[g1g2]
GI-D468     LVKYKTPQPW PSEELIADQC PLPGYHAGVE YTTQAIWDYY   276

GII-K74     LVKYKTPQPW PNEGLIADQC PLPGLADVSF YPYQAIWDYY   276

IKVESIRPAN  WTTKSKYGQA RLGSFYIPSS LRQINVSHVL FCSDQLYSKW   326
IKVEITRPKN  WTSYAQYGNA RLGSFFIPPH VRK-NFTHVL FCSDQLYAKW   325
AKIENIRPAN  WTSSKLYGKA RMGSYYIPKR LRNINNTHIL FCSDVLYSKW   326

YNIENTIEQN  ERFLLNKLNN LTSGTSVLKK RALPKDWSSQ GKNALFREIN   376
YNIENTLLKN  EELLQKKLNN LTELTSLLKK RALPRTWTTQ GKNNLFRNIT   375
YNLQNSILQN  ENELTKRLSN LT-IGNKLKN RALPYEWAKG GLNRLFRNIS   375

VLDICSKPES  VILLNTSYYS FSLWEGDCNF TKDMISQLVP ECDGFYNNSK   426
                           b-BAK56[g1]
VLDVCNRPEM  VLLLNISYDL FSLWEGDCNY TKDKISEIVP QCKGFYNNSK   425
                           b-BAK56[g1] BAK82[g1]
VLDVCSRPEM  VLLLNKTYYT FSLWEGDCNI TRYNVNETVP ECKDFPHRR-   424

WMHMHPYACR  FWRSKNEKEE TKCRDGETKR CLYYPLWDSP ESTYDFGYLA   476
                 c-BAD551[g2] BAK55[g1g2] BAK74[g1g2]
WMHMHPYACR  FWRNKNEKEE TKCDGRDDNK CLYYPLWDSP EATYDFGFLA   475
-FNDHPYSCR  LWRYREGKEE VKCLTSDHTR CLYYPEYSNP EALFDFGFLS   473

d-BAK132[g1]
YQKNFPSPIC  IEQQKIRDQD YEVYSLYQER KIASKAYGID TVLFSLKNFL   526
              e-BAK56[g1]
YQNNFPAPIC  ISSKQIRQQD YEVYSIYQEC KLASRIHGID SVLFSLKNFL   525
              e-BAK56[g1]
YMRNFPGPQC  IESTSIRQQD YEVYSIYQEC KLASKTYGID SVLFSLKNFL   523
```

920 Figure 3. The SFV SU blocks nAbs without affecting viral entry

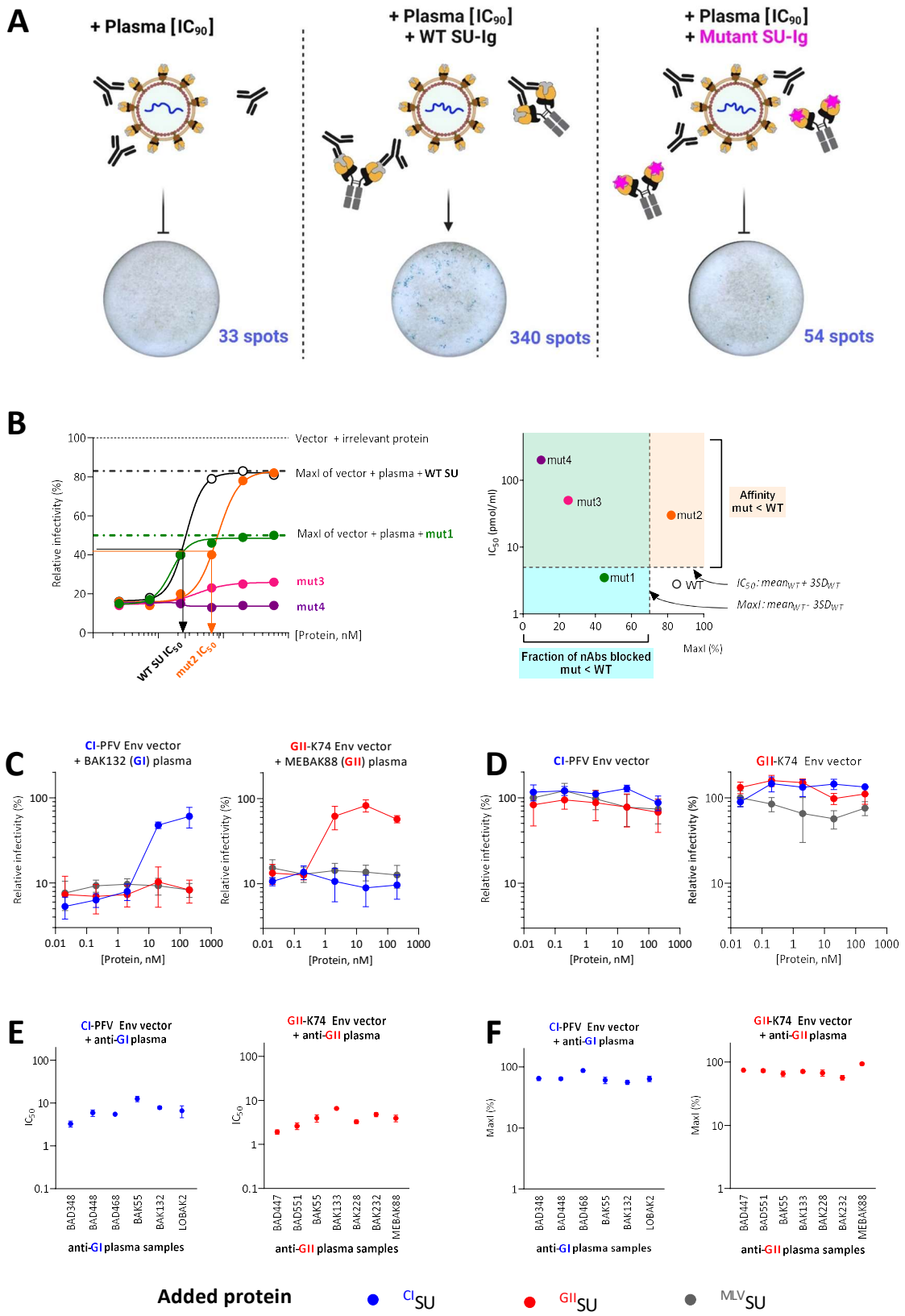

921

922

923 Figure 4. SFV-specific nAbs recognize glycans on SUvar

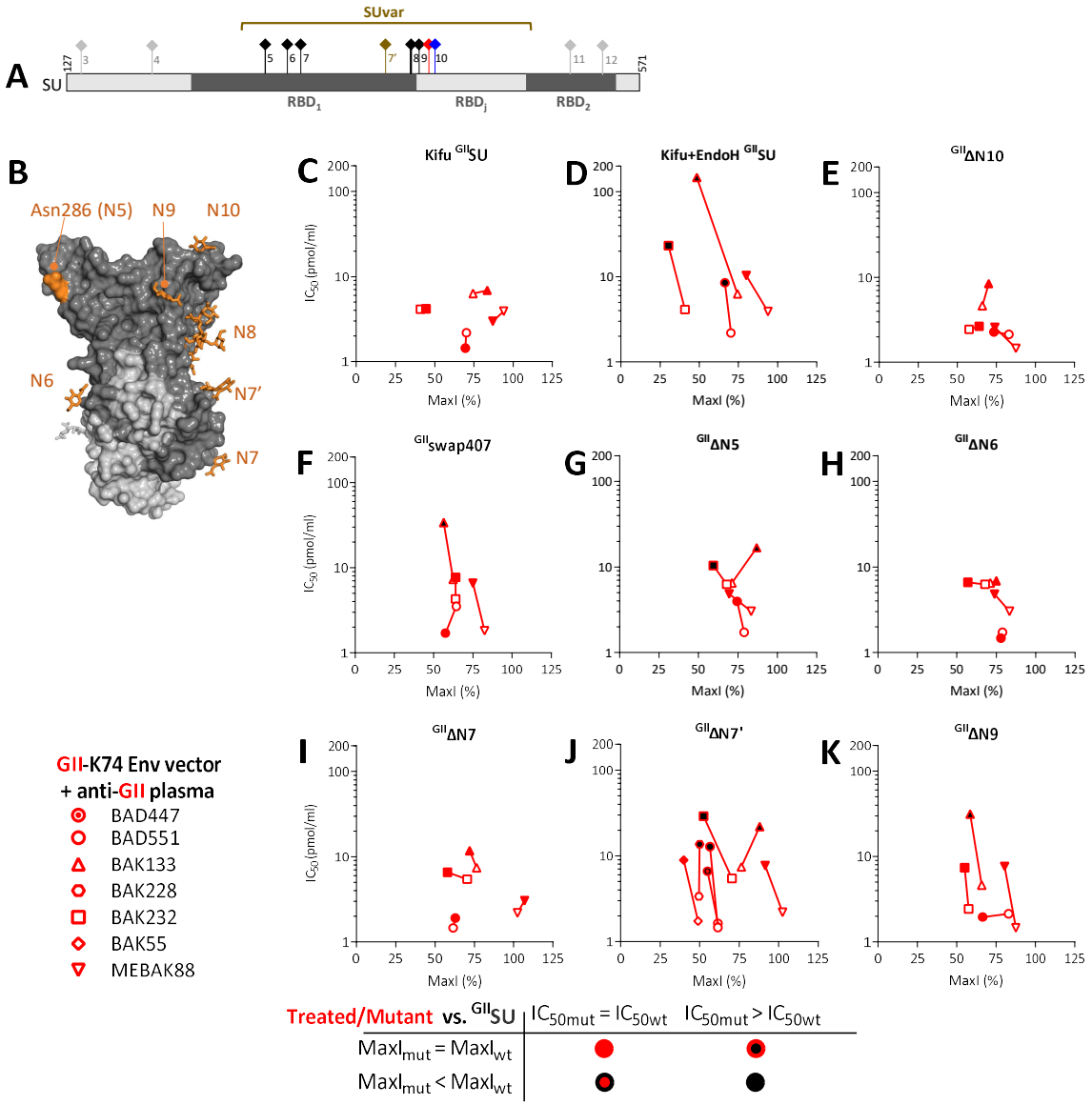

924

925

Figure 5. Most SFV-specific nAbs recognize the RBDj domain

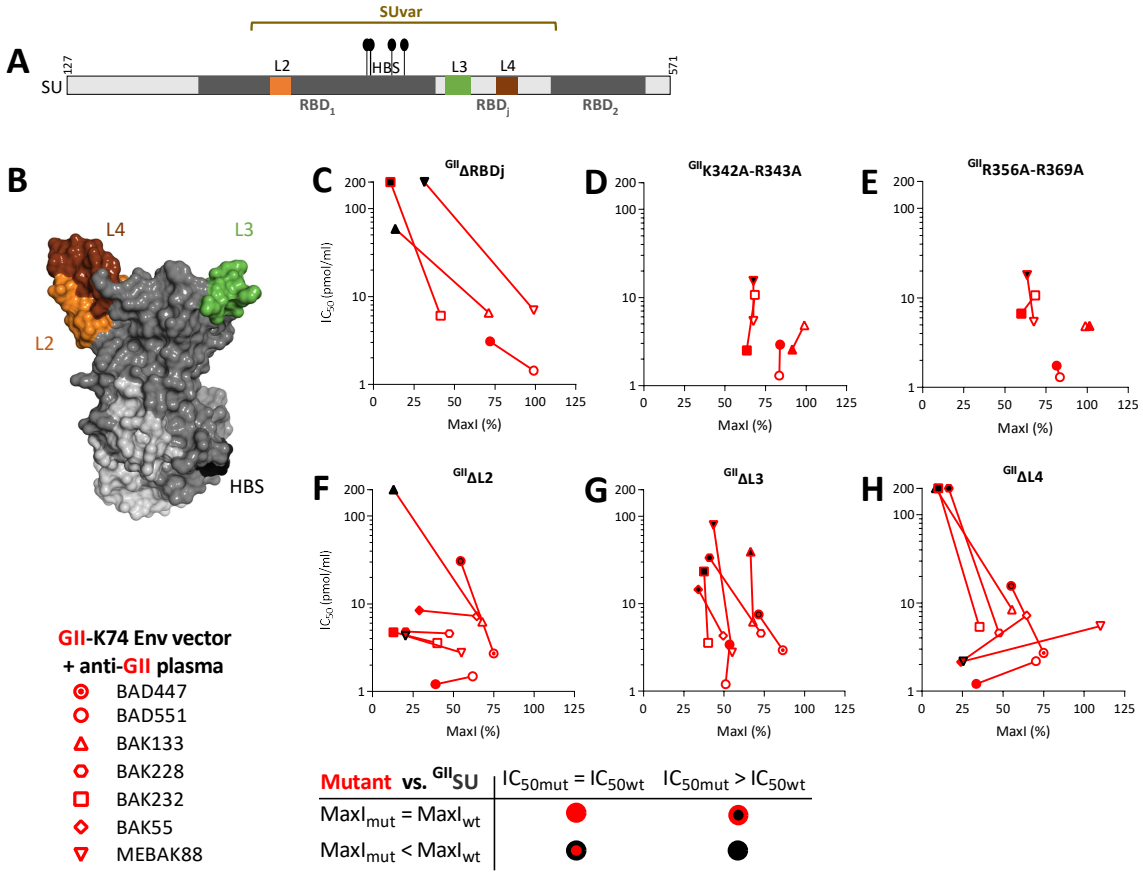

Figure 6. Epitope disruption by glycan insertion reveals additional nAb recognition sites

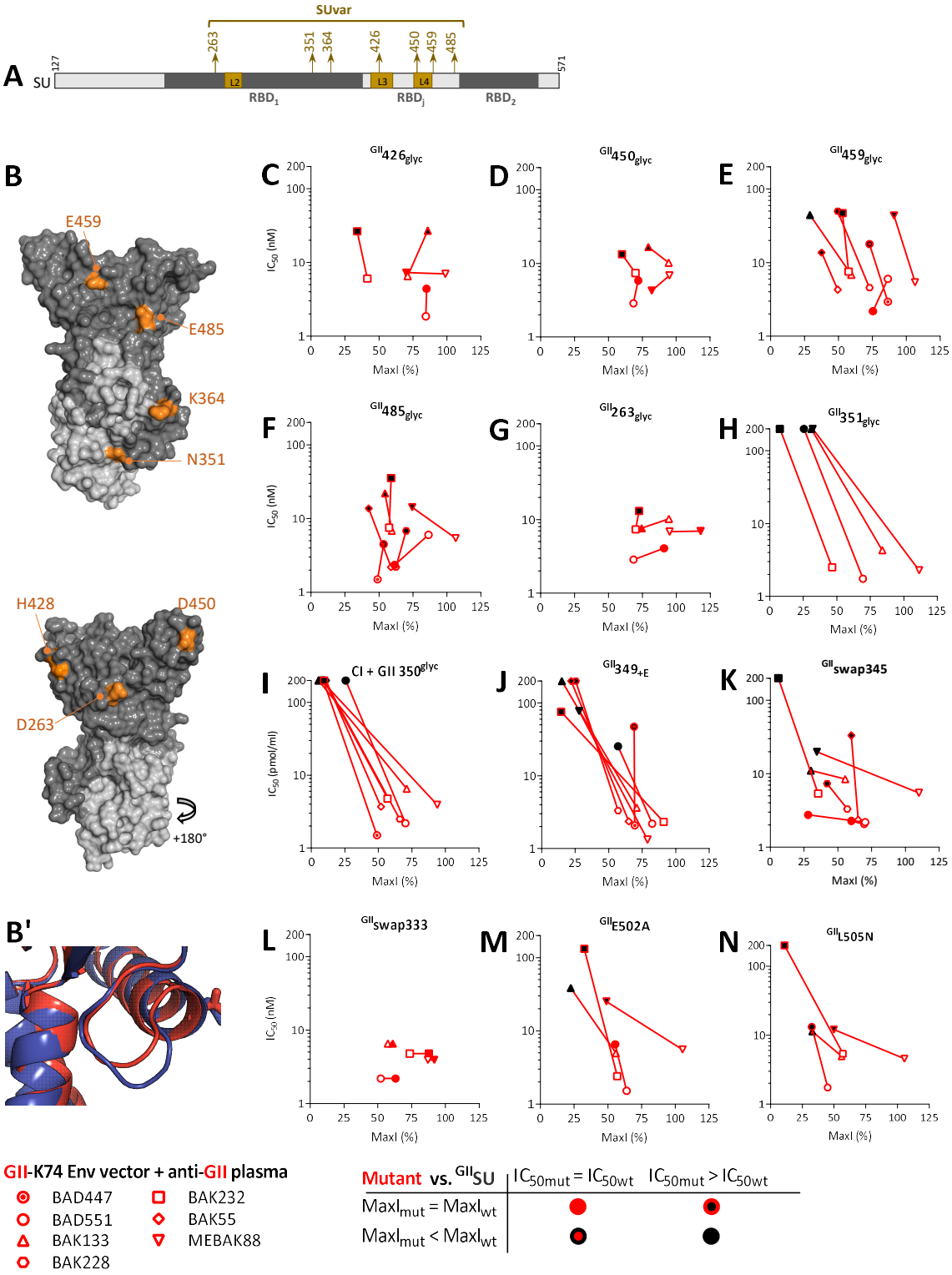

Figure 7. GI and GII-specific nAbs target different epitopes

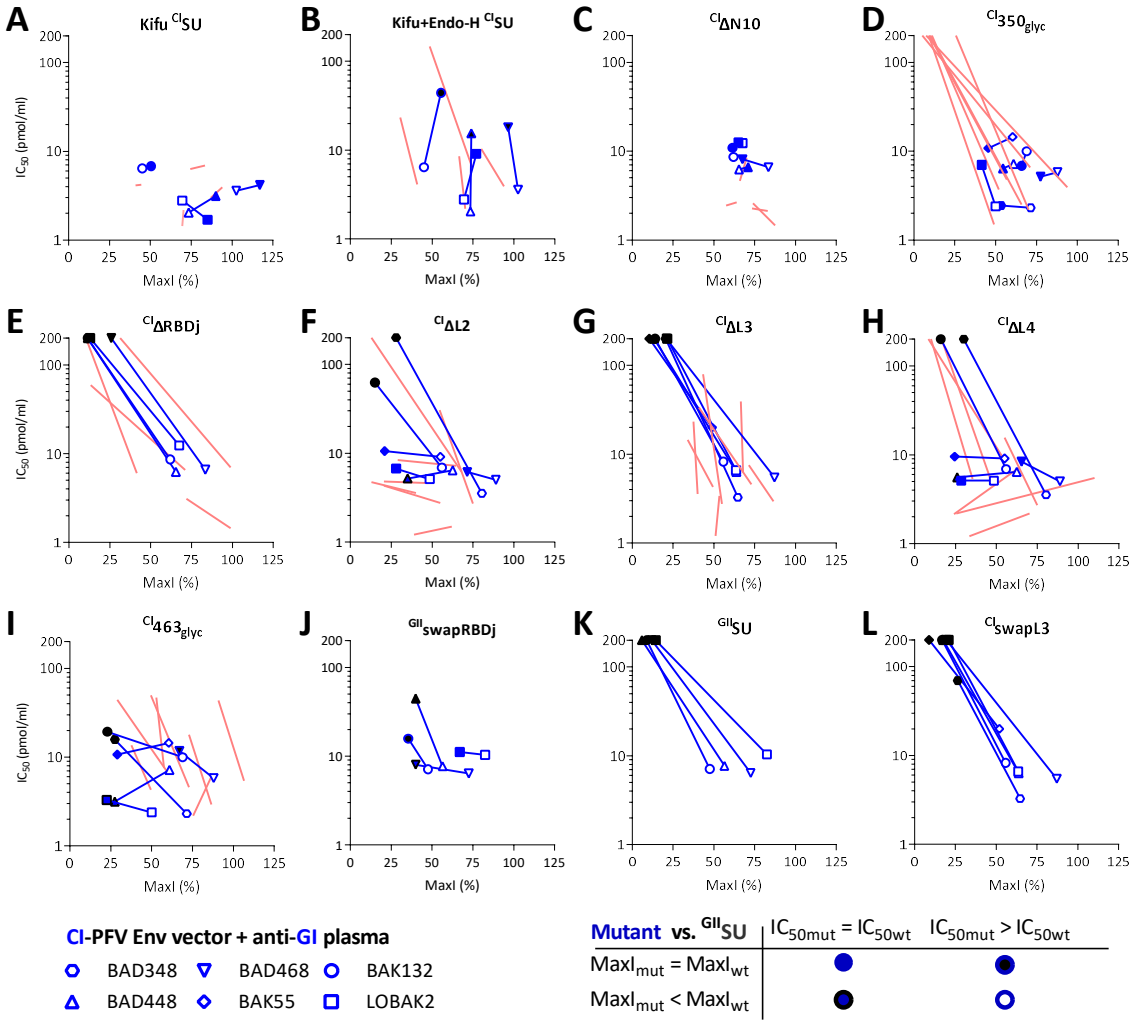

Figure 8. Most samples contain nAbs that recognize several epitopic regions on SUvar

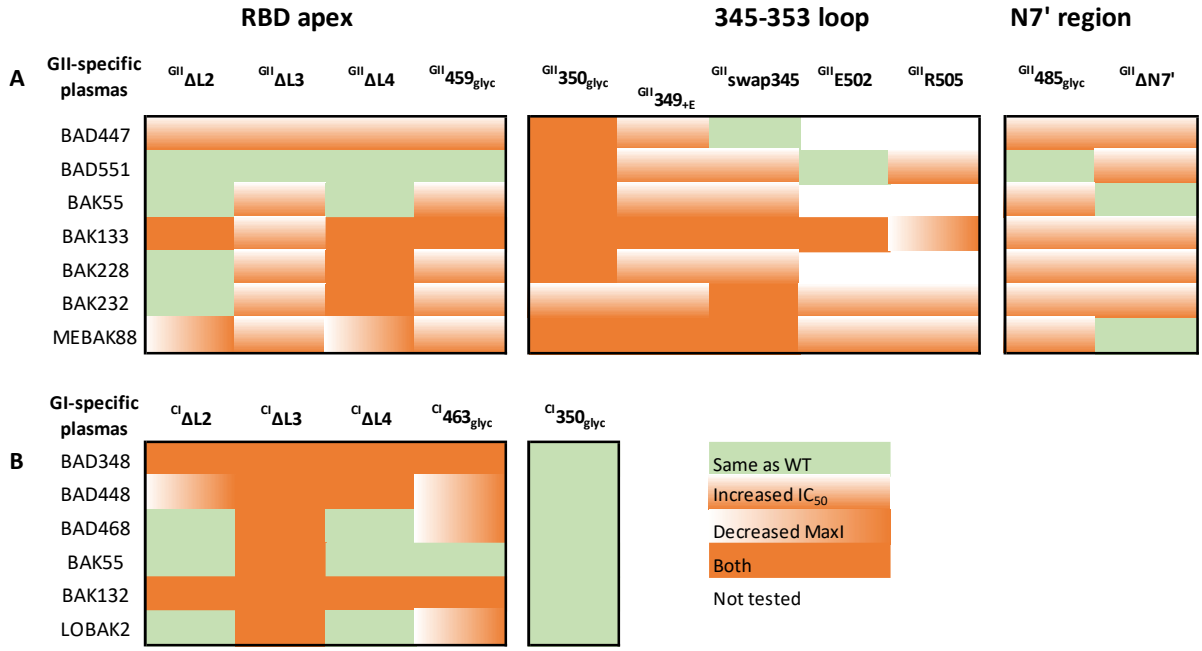

Figure 9. nAbs target epitopic regions involved in SU binding to susceptible cells or required for viral infectivity

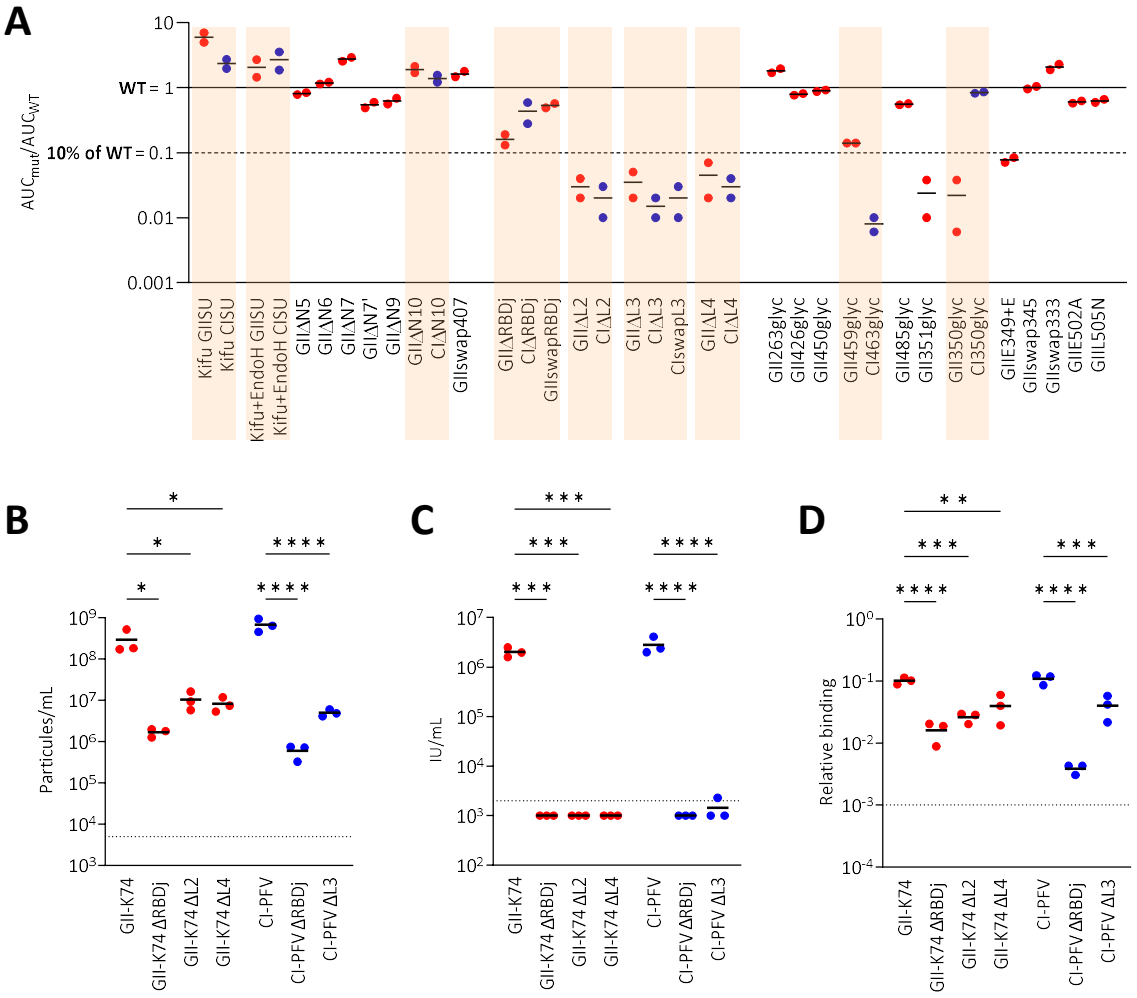
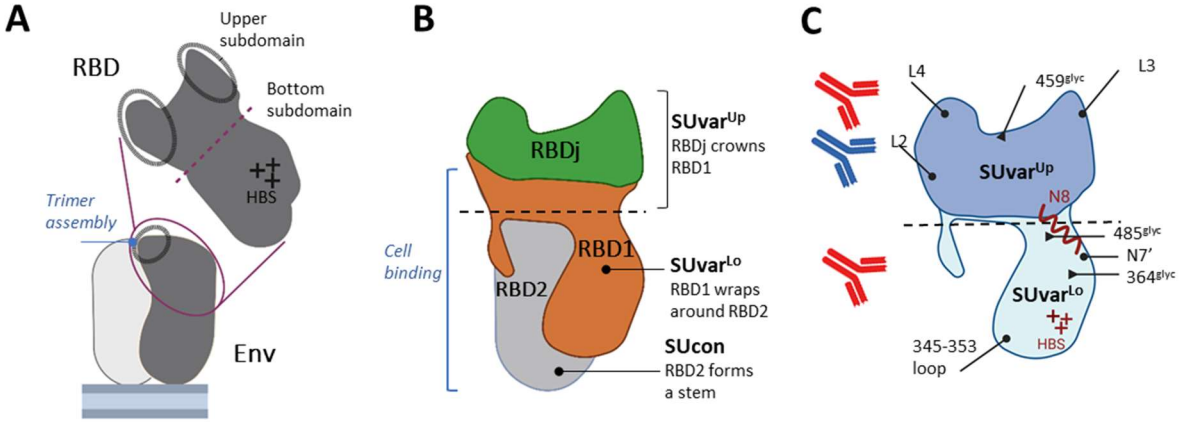
Figure 10. Schematic summary of current knowledge on SFV Env